)

Study of Scene-Based Nonuniformity Compensation in

Infrared Focal Plane Arrays

by

Laura S. Juliano

B.S., Electrical Sciences and Engineering
Massachusetts Institute of Technology, 1995

Submitted to the Department of Electrical Engineering and Computer Science

in Partial Fulfillment of the Requirements for the Degree of

Master of Engineering in Electrical Engineering and Computer Science

at the Massachusetts Institute of Technology

May 1996

Copyright 1996 Laura S. Juliano. All rights reserved.

Author _____

Department of Electrical Engineering and Computer Science
May 10, 1996

Approved by _

Kenneth I. Schultz
Technical Supervisor, MIT Lincoln Laboratory

Certified by _

David H. Staelin
sis Supervisor

Accepted :

Morgenthaler
Chairman, Department Committee on Graduate Theses

Study of Scene-Based Nonuniformity Compensation in Infrared Focal Plane Arrays

by

Laura S. Juliano

Submitted to the Department of Electrical Engineering and Computer Science

May 10, 1996

In Partial Fulfillment of the Requirements for the Degree of
Master of Engineering in Electrical Engineering and Computer Science.

Abstract

Infrared Focal Plane Arrays (FPAs) are used in a wide variety of military and industrial applications which require the collection of low noise, high resolution images. In many of these applications, the dominant noise results from array response nonuniformities. For low noise applications (e.g., detection of low contrast, unresolved targets), correction for the nonuniform array response is critical for achieving the maximum sensitivity of these arrays. Two classes of techniques for reducing the effects of nonuniformity are source-based compensation, which employs the use of one or more uniform calibrated sources, and scene-based compensation, which uses scene data to estimate nonuniformity.

This thesis evaluates the performance of both source-based and scene-based compensation techniques using experimental sensor data. Array nonuniformities were first characterized and then used to predict the performance of the different compensation techniques. Two-point source-based nonuniformity compensation techniques, which use uniform calibration sources at two temperatures, were applied to blackbody images over a wide range of temperatures and shown to reduce spatial variations to an average of 0.82 sensor counts (0.03°C). One-point compensation techniques performed as well only near the calibration temperature; over the wide temperature range, variations averaged 14.7 sensor counts (0.5°C). Scene-based algorithms were evaluated using measured IR images and were found to decrease spatial variation below that of the two-point compensation technique, from 43 counts to as low as 17 counts, as a result of the algorithms' clutter rejection capabilities. The effects of scene-based techniques on target suppression were not evaluated as a part of this thesis.

VI-A Company: MIT Lincoln Laboratory
Thesis Supervisor: David H. Staelin
Title: Assistant Director, Lincoln Laboratory

Acknowledgments

Table of Contents

List of Figures

1 Introduction

1.1 Problem Statement

Nonuniformity in infrared focal plane arrays (FPAs) results in fixed pattern noise which limits infrared system performance. The methods which are commonly used to reduce fixed pattern noise can be separated into two main categories: source-based and scene-based nonuniformity compensation techniques.

There have been a number of studies of source-based compensation techniques, but there has been considerably less work in evaluating and analyzing scene-based techniques. This thesis will investigate scene-based nonuniformity compensation methods; specifically, scene-based compensation techniques are analyzed to determine the conditions for which a specific level of spatial uniformity can be achieved. This information can be used to determine reasonable conditions for data collecting and subsequent processing.

To this end, nonuniformity characteristics are examined using experimental sensor data. A laboratory setup consisting of an infrared imaging system, blackbody source, and simple targets was used to obtain test data. The data are used to highlight aspects of nonuniformity and provide motivation for compensation techniques.

Source-based methods are developed and applied to experimental data. These performance results serve as a baseline for comparison for the scene-based techniques. The capabilities of one specific scene averaging technique are examined for a variety of

backgrounds as a function of the spatial frequency and contrast of the background scene. In addition, data collected by one or more operational sensors are used as another test of the various compensation methods. The combination of theoretical and experimental work provides an analysis of scene-based compensation techniques.

1.2 Thesis Organization

This thesis consists of six chapters which develop nonuniformity characteristics and an analysis of nonuniformity compensation. The first chapter provides a brief introduction to the goals and organization of this thesis.

The second chapter gives an overview of infrared focal plane arrays and introduces the problems of nonuniformity. This chapter also introduces the concepts of scene-based and source-based nonuniformity compensation.

Chapter 3 consists of an analysis of the spatial and temporal characteristics of focal plane array nonuniformity. It also addresses nonuniformity measurement issues and describes the experimental setup used to obtain sensor data.

Chapter 4 concentrates on the source-based nonuniformity compensation techniques. This serves as the basis of comparison for the evaluation of the scene-based compensation techniques.

Chapter 5 introduces scene-based algorithms and discusses algorithm implementation and performance. The results are compared to the performance of the source-based compensation techniques.

The final chapter presents a summary of the thesis and discusses potential future work.

2 Background

The goal of this chapter is to introduce the reader to focal plane array technology and to provide a context for the problem of nonuniformity compensation. First, an overview of infrared imaging applications is presented. Nonuniformity and its relation to detector performance is then discussed. In addition, motivation for nonuniformity compensation is developed. The chapter concludes with a general overview of the source-based and scene-based compensation techniques.

2.1 Overview

Infrared systems have long been of interest in military systems and more recently in commercial applications. This interest is based on the desire to detect, recognize, classify, or identify objects by their emission characteristics. Objects at or near room temperature (295K) have a peak emission at 9.8 μm, as determined by the Wien Displacement Law for peak radiation. Hot objects, such as the plume from a jet aircraft, approximately 650K (Hudson, 1969) have a peak emission at 4.5 μm. These two classes of objects have led to the interest in infrared technology, more specifically to mid-wave (3-5 μm) and long-wave (8-12μm) spectral bands. These bands are even more significant when one observes the atmospheric windows associated with these two infrared spectral bands. The atmosphere has very high transmission for both the mid-wave and long-wave bands, less the CO_2 absorption band from 4.2 to 4.5 μm and the H_2O absorption band from 9.5-10.2 μm.

Initially, infrared imaging technology consisted of a small number of detectors which were scanned across an image. Since these scanned linear arrays had a small number of detectors, it was relatively easy to fabricate detectors with matching characteristics. There are drawbacks associated with these scanning systems; additional hardware and optics are required to implement the scanning mechanism. For each frame of data, the detector array must scan across the image. This limits the pixel integration time, which reduces system sensitivity.

As the fabrication technology advanced, staring focal plane arrays with large numbers of detector elements were developed. As these arrays do not require scanning, they provide for significantly increased integration times, and therefore increased sensitivity. Since there are a large number of detector elements, the quality of fabrication techniques is crucial to the development of large, uniform arrays; nonuniform production techniques can result in nonuniform array response. Such array nonuniformities may in fact limit sensitivity; spatial variations in the array response can obscure the target signature, which reduces system detection performance. The problem is further complicated, as the spatial variations in array response can vary with time. Any technique to compensate for nonuniform array response must consider how the response varies during the time of interest.

Since the development and performance of FPA-based infrared systems have been limited by array nonuniformity, nonuniformity compensation techniques are generally required to achieve the full potential of staring focal plane arrays. These techniques are classified as either source-based or scene-based techniques. Source-based techniques

employ the use of one or more uniform radiation sources to calculate compensation coefficients. Such techniques can be complex to implement since they require uniform sources and additional hardware to make the compensation measurements. If the source radiation or temperature characteristics are known, source-based techniques have the potential to provide calibrated image data; the sensor output can be mapped from counts to absolute temperature or radiance values. Scene-based compensation techniques use image data to calculate compensation coefficients. Consequently, scene-based techniques have a potential to provide a simple alternative to source-based techniques. For many applications of practical interest, such compensated relative measurements are sufficient (e.g., target detection).

2.2 Infrared Imaging Applications

Infrared focal plane arrays, both scanning and staring two-dimensional arrays, have a wide variety of applications. The specifics of the system application affect the choice of the FPA, and influence the choice of the nonuniformity compensation approach. Various applications of interest are described below.

In infrared search and tracking (IRST) applications, the system is generally used for long-range surveillance, early target detection, and tracking. The normal system mode of operation is characterized as "track-while-scan". The detector array is scanned across an inertially stabilized volume in space. Single or multiple targets are detected and tracked in subsequent frames while the system continues to scan the prescribed inertial volume. Tracking is maintained through frame to frame correlation of detections. Due to the long

range operational requirement, the targets of interest are unresolved, typically less than the size of a pixel (detector element). Therefore, high sensitivity and resolution are required in IRST applications.

Infrared missile warning systems (IMWS) have the same unresolved target, track-while-scan functionality as IRST systems. In the case of aircraft-based missile threat warning systems, a wide-field-of-view sensor with a two-dimensional staring array is used to detect the unresolved missile targets (Kruer, Scribner, and Killiany, 1987). The goal of the system is to achieve rapid target declaration, with a low false alarm rate, in order to either avoid the missile or employ countermeasures to defeat the missile.

In the case of an infrared missile seeker application, the detector is mounted within a gimbal in the nose of the missile. The objective is to acquire and intercept a single target. Generally, the infrared seeker is cued to a target area and must rapidly acquire the initially unresolved target, since engagement times can be on the order of seconds. Missile seekers typically employ single target detection and tracking, as opposed to multiple target tracking.

Forward looking infrared (FLIR) sensors are traditionally used for air-to-ground target recognition and tracking for weapon delivery. In this case, the target is centered in the field-of-view of the sensor, and the system tracks a single target. FLIR systems are often equipped with boresighted laser range finders for weapon guidance. Unlike the missile seeker applications, the targets are highly resolved and the output signal is intended to be viewed and interpreted by a human operator. Advanced systems couple the output

signal to automatic target recognition functions which automate the weapon delivery process.

While each of these applications has its own set of requirements for infrared sensor performance, the subsequent system characteristics affect the implementation of nonuniformity compensation algorithms. Although all applications can potentially benefit from nonuniformity compensation, the efficacy of the compensation algorithms varies with the application. With IRST applications, for example, compensation may be applied after several frames of data. Therefore, a compensation algorithm that requires multiple frames of data may not adversely impact sensor performance. However, in seeker applications where the time of engagement is very short and access to an infrared reference source difficult to implement, compensation needs to occur after just a few frames without the benefit of a calibrated reference. In the case of FLIR systems, where a human observer is involved in the infrared scene interpretation, precise nonuniformity compensation is less important. Compensation cannot be considered without regard to sensor application.

2.3 Generic FPA Imaging System

IRST and IMWS represent an emerging class of infrared systems where the objective is to detect unresolved targets. Figure 2-1 shows the general image processing steps used in these infrared system applications. The FPA sensor images either a background scene, which may contain potential targets, or a uniform calibrated reference source. Following image acquisition, a high-pass filter can be used to accentuate high spatial frequency components (as associated with an unresolved target) relative to a low

spatial frequency background (e.g., scene clutter). A threshold test is then applied to the high-pass filtered image to test for the presence of targets. This filtering method selects pixels that do not match the underlying correlation of the background scene; the target is assumed to have high spatial frequency relative to the background. Nonuniformity tends to have high spatial frequency components; in this respect, nonuniformity characteristics are very similar to target characteristics and therefore will not be removed by high-pass filtering. If the nonuniformity is not corrected by the use of compensation algorithms prior to target detection, the detection capabilities of a system will be greatly diminished, as the nonuniformity may cause false alarms.
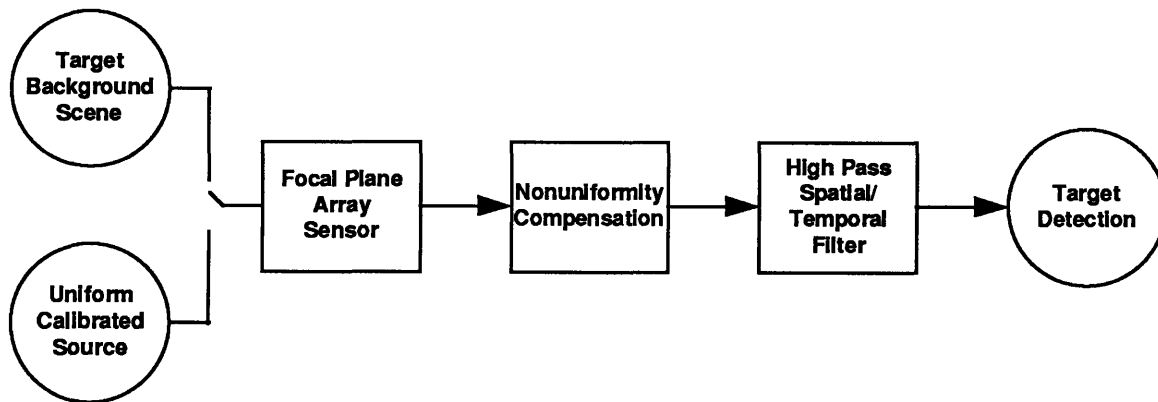
Figure 2-1: Image Processing Block Diagram

2.4 Introduction to Focal Plane Arrays

Originally, infrared detectors consisted of either a single detector element or a small linear array of detector elements that were scanned across a scene to obtain an infrared representation of the scene. Scanning sensors using these detector configurations

were limited in both resolution and sensitivity, since they typically had a limited dwell time and large detector size. As detector technology matured, large numbers of detector elements could be fabricated as part of a two-dimensional FPA. The array of detectors is coupled to a multiplexer/preamplifier readout circuit.

Two-dimensional staring FPAs, consisting of thousands of detectors, have a number of potential advantages over systems with scanned linear arrays. The staring array design allows economical high-density packing of detectors on the substrate, and allows for future, advanced signal processing on the focal plane. In addition, infrared systems employing staring FPAs have increased sensitivity due to longer integration times, higher frame rate capabilities and simpler optics.

There are fabrication issues which affect the performance characteristics of FPAs. The nonuniformity of the detector arrays is often the limiting factor in system performance. Noise can also be introduced in the readout circuitry, which transfers the detector signals off the focal plane. Charge transfer efficiency variations across the array are also a source of nonuniformity. Another source of noise is cross talk, where signals from one detector affect the readout circuitry for nearby detectors.

2.4.1 FPA Detector Materials

There are a number of issues to consider when selecting infrared detector materials. The detector material must operate in the desired spectral band, for example, either mid-wave infrared (MWIR) or long-wave infrared (LWIR). The detector material must have acceptable electronic properties over an operationally feasible temperature regime. The fabrication technology must be mature enough to produce uniform arrays;

17

processing which is silicon-based is more developed and controllable than processing which involves less common materials.

Typical applications for infrared FPAs require detectors that operate in either the MWIR or LWIR. The MWIR consists of the spectral band ranging from 3-5 μm. The LWIR includes wavelengths in the 8-12 μm spectral band. The operating region has a direct relation to the required bandgap of the detector material. The relationship between bandgap energy and spectral operating region is given by,

$$E = \frac{1.24}{\lambda}[eV],$$

where E is the bandgap energy and λ is the maximum wavelength in the spectral band. This relation requires the detector material to have a bandgap energy of approximately 0.1 eV for LWIR detectors and 0.25 eV for MWIR detectors.

In order to reduce dark current in the detector, the FPA is operated at a low temperature. The temperature of operation depends on the allowable array noise, but is typically 77K, for infrared sensors. Over the detector spectral band, the quantum efficiency of a detector is a measure of how well the material converts incident radiation to electric charge. High quantum efficiency detectors (e.g., InSb and HgCdTe) have quantum efficiency values over 60%, while low quantum efficiency detectors (e.g., PtSi, IrSi) have quantum efficiencies less than 1% (Cantella, 1992).

Producability is also a key issue in focal plane array development. In order to fabricate a uniform array, the process must be well controlled. The process uniformity places a practical limit on the size of the focal plane array.

Three main detector materials, which satisfy the requirements for good infrared detection, are platinum silicide (PtSi), indium antimonide (InSb), and mercury cadmium telluride (HgCdTe). Platinum silicide and indium antimonide are limited to mid-wave detection. While platinum silicide is advantageous because it is silicon-based, and the technology is very mature, this material has low quantum efficiency and must be operated at very low temperatures. Indium antimonide has a high quantum efficiency and advances in InSb processing technology have resulted in high quality FPAs. Mercury cadmium telluride, with its variable bandgap, can be operated in either the mid-wave or long-wave infrared bands. The bandgap of HgCdTe is a function of composition and therefore any nonuniformity in composition creates nonuniformity in spectral response. HgCdTe has a significantly more complex fabrication procedure, as compare to PtSi or InSb, particularly in long-wave applications, which results in reduced uniformity. For many applications, this drawback is outweighed by its high quantum efficiency and low noise operation. The data used in this investigation were obtained from both InSb and HgCdTe arrays.

2.5 Nonuniformity in Focal Plane Arrays

In many cases, nonuniformity is the limiting factor in the detection performance of infrared focal plane arrays. To understand why this is the case, we must examine the sources and characteristics of array nonuniformity. The goal of this section is to give the reader a general sense of the importance of nonuniformity compensation. More specific characteristics of nonuniformity are analyzed in Chapter 3.

Nonuniformity in FPAs arises from a number of sources. Differences in the dimensions and geometry of the individual detectors cause differing responses from one detector to another. Variations in material composition affect detector quantum efficiency and spectral response. In HgCdTe arrays, for example, changes in composition of the detector material result in detectors with varying bandgap. This causes a variation in the maximum cutoff wavelength, which results in nonuniformity in spectral response. Nonuniformity also occurs when there is a variation in the coupling of the detector to the readout mechanism. Finally, temperature variations across the array, which come from uneven cooling of the focal plane array, affect the detector response. It is important to understand that the sources of nonuniformity have different spatial and temporal characteristics. In general, periodic nonuniformity compensation is required to maximize array uniformity. This drift in focal plane array response presents special problems with nonuniformity compensation.

The following images in Figure 2-2 demonstrate some of the important characteristics of sensor nonuniformity. The image on the left is a raw image taken with a HgCdTe sensor, where the background is a desert scene. The image on the right is the same image, after nonuniformity correction. The scene detail is greatly increased after compensation.

(a)   (b)
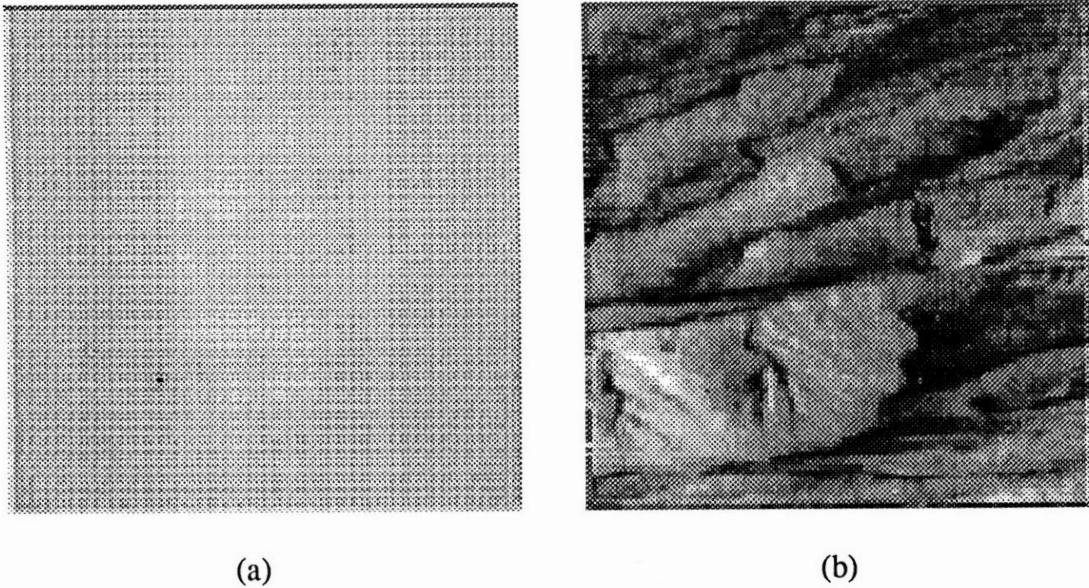
Figure 2-2: Infrared image from an HgCdTe sensor a) before nonuniformity compensation and b) after nonuniformity compensation

As is evident in the uncompensated image, the nonuniformity completely obscures the scene data. In this example, the scene information consists of small perturbations about the much larger nonuniformity. This tends to be a problem in infrared imaging, because infrared scenes typically have low contrast.

Although the magnitude of the nonuniformity poses a serious problem, it is the spatial frequency characteristics of the nonuniformity that present the greatest problems with respect to performance. Simple high-pass filtering will not remove the non-uniformity present in the above images, since the nonuniformity has considerable high frequency components.

2.6 General Algorithms for Nonuniformity Compensation

The two main classes of nonuniformity compensation algorithms are source-based and scene-based compensation. An overview of these techniques is presented here and the algorithms are explored in greater depth in Chapters 4 and 5. See Table 1 for a qualitative overview of source-based and scene-based methods.

	Advantages	**Disadvantages**
Source-Based	Absolute calibration Good performance near calibration temperature	Recalibration required Poor performance away from calibration temperature
Scene-Based	No blackbody required Adaptive algorithm	Relative temperature calibration Generally correct offset only

Table 1: Relative Merits of Compensation Techniques

Source-based nonuniformity compensation techniques commonly employ one or more uniform blackbody sources. These blackbody sources serve as calibration references from which compensation coefficients are derived. The most common source-based technique is a two-point correction scheme, which compensates for offset and gain variations from pixel to pixel. In this technique, the sources are operated at temperatures which span the scene temperatures anticipated in normal system operations.

Source-based nonuniformity compensation must be embedded in the system to accurately address drift in FPA response, an initial factory calibration is not sufficient. Therefore, periodic recalibration within the infrared system is required for accurate compensation. The implementation of the blackbody reference within the system can be impractical or costly in many applications; the system needs more complicated optics in order to view the blackbody and a place in a the system to locate the reference sources.

Scene-based compensation uses scene data to approximate observations of a uniform temperature source, thus simplifying the imaging system. Compensation coefficients are generally calculated from some form of spatial averaging over diverse scenes. This can be accomplished in a variety of ways, including spatial or temporal filtering, angle dither, and image defocus. Unlike source-base calibration, scene-based compensation is a relative calibration. This is not, however, a problem in IRST or IMWS applications where the temperature difference between background scene and target objects, as opposed to the absolute temperature, is the quantity of interest.

3 Nonuniformity

The goal of this chapter is to gain an understanding of the sources of nonuniformity and the spatial and temporal characteristics of nonuniformity. This will be important later in evaluating nonuniformity compensation algorithms. This chapter will investigate some of the general characteristics of nonuniformity in focal plane arrays. Experimental data will be used to illustrate some of the key features of sensor nonuniformity.

3.1 Experimental Setup

The majority of the data analyzed in the next two chapters were obtained with the Cincinnati Electronics IRC-160ST imaging system, which has a 160x120 InSb array. The IRC-160ST has a standard 50mm EFL (Effective Focal Length) lens that provides a total field-of-view of 9.1° in azimuth by 6.8° in elevation and a nominal pixel resolution of 1 milliradian. An additional 200mm EFL lens can be attached, providing 2.3° x 1.7° field-of-view and a 0.25 mrad pixel resolution. The detector/multiplexer array in the camera is cooled to 78K with a mechanical Stirling Cycle microcooler (Cincinnati Electronics 1993).

The laboratory setup for the camera is shown in Figure 3-1. The camera was arranged to view a target that was projected at the focus of a collimator. The target that was primarily used was a flat target that transmitted the radiation of the 12 inch blackbody that was behind it. The blackbody temperature ranged from 10°C to 60°C.

The digital data from the camera were transferred to a Sun SPARC workstation via a digital video interface board (frame grabber). The frames of data can be displayed as well as written to a file. The images were obtained and processed using the Interactive Data Language (IDL). Some of the code written for processing images in this thesis was code developed in the Air Defense Systems group at Lincoln Laboratory for the Airborne Infrared Imager (AIRI).
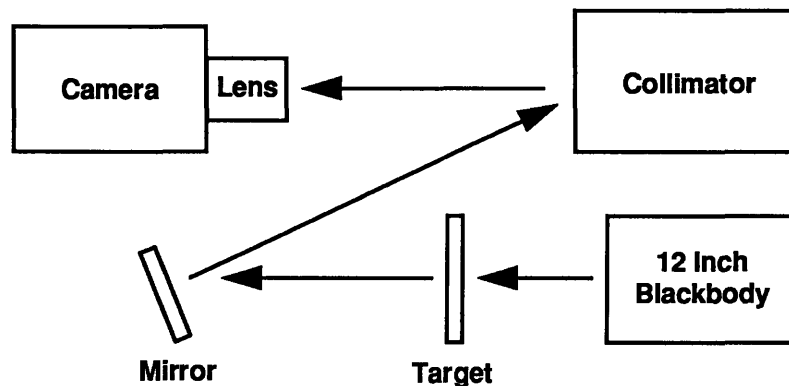
Figure 3-1: Laboratory setup for CE camera

3.2 General Nonuniformity Characteristics

In Chapter 2, the image from a HgCdTe sensor before nonuniformity compensation helped to illustrate some characteristics of nonuniformity in focal plane arrays. The nonuniformity was significant compared to the background image and it had high spatial frequency components. In this chapter, these characteristics will be quantified. The data used in this section is primarily imaged blackbody data. Since the blackbody provides uniform radiance, all variations in the output images will be caused by

nonuniformity. As an example, Figure 3-2 is a histogram of the output of the individual

detector element response in the CE InSb array to a 25°C blackbody.

Temperature (degrees C)
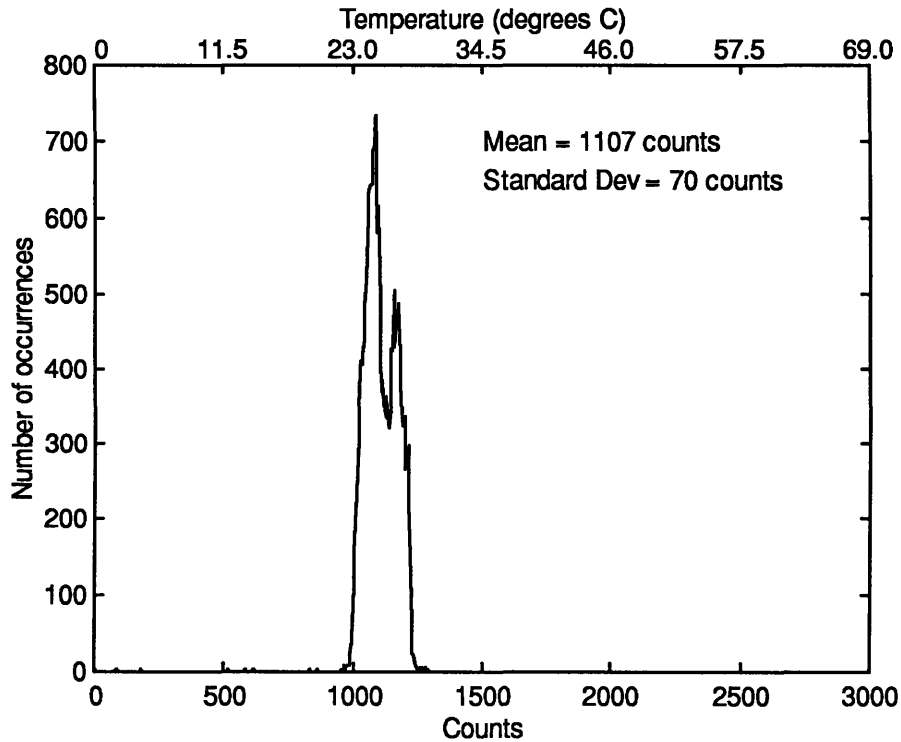
Figure 3-2: Histogram of InSb response to 25°C blackbody

Nonuniformity in focal plane arrays can be described as a combination of an

additive or offset term, a multiplicative or gain term, and higher order terms. The output

of each detector, x(t), including the nonuniformity terms, can be written as a function of

the scene radiance, r(t), as follows:

$$x(t) = a(t) + b(t)r(t) + f(r, t),$$

where x(t) is the output of the detector, a(t) is the offset term, b(t) is the gain term, and

f(r,t) represents the higher order terms. The time dependence of the nonuniformity terms

is examined later in the chapter. In this thesis, the high order nonuniformity terms are neglected.

The additive nonuniformity component a(t), which is not a function of scene radiance, comes from variations in dark current, charge-transfer efficiency, and variations in the readout mechanism. This offset term dominates at very low radiance values.

The multiplicative nonuniformity term, b(t)r(t), is the term which is a function of exposure. This results from variations in the responsivity from detector element to detector element and from photon noise, which is proportional to the square root of exposure. The effects of the gain and higher order terms increase as background radiance increase. The relative importance of correcting for gain and offset variations is an issue that will be addressed when evaluating compensation algorithms.

3.2.1 Sensor Response as a Function of Scene Radiance

One important measurement of an array is how the response of the array varies with scene radiance. Figure 3-3 demonstrates the mapping between background temperature and the output of the InSb detector array, measured in counts. The array was used to image a blackbody over a range of temperatures. This gives an indication of the relationship between scene temperature and output counts of the detector system. This plot can be used as calibration data, that is, it provides the information necessary to convert sensor counts to temperature. This will be useful in converting the variance of the response in counts to an apparent temperature variance.
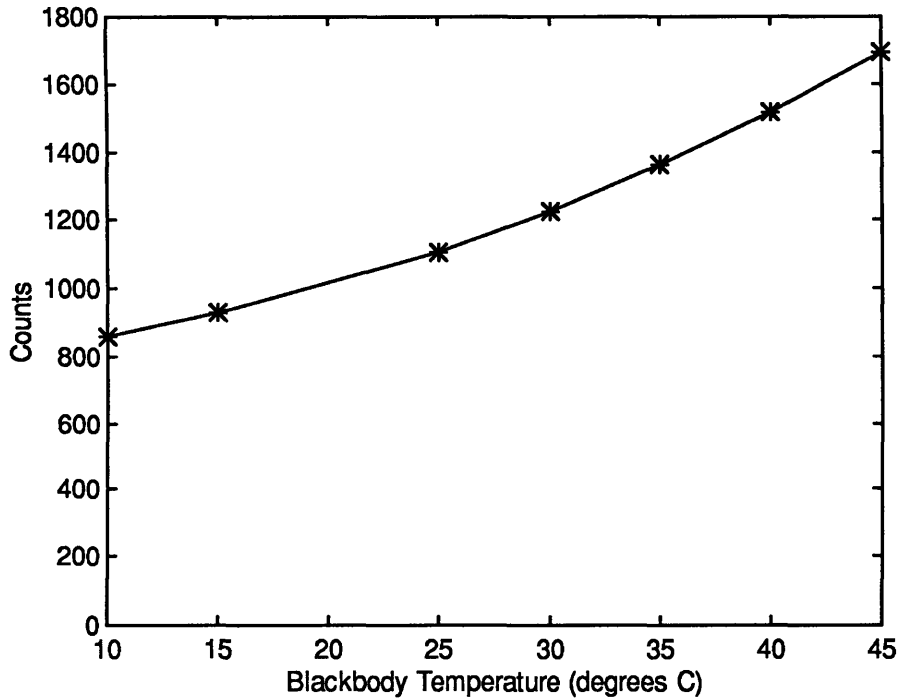
Figure 3-3: Mean of InSb array response as a function of blackbody temperature

To verify that the above response as a function of temperature is as expected, we use Planck's law, which gives the spectral distribution of the blackbody radiance as a function of temperature,

$$R(\lambda) = \frac{37413}{\lambda^5 (Exp(\frac{14388}{l\lambda}) - 1)} \ [W\ cm^{-2}\mu^{-1}].$$

Integrating the above equation over the spectral band in which the CE camera operates, 2.2μm to 4.7μm, will give the relationship between the radiance and the temperature source. Table 2 lists the results of the integration for the temperatures of interest. Using these data, we can plot the sensor output (in counts) against the radiance of the blackbody source. Figure 3-4 indicates that the sensor output is a linear function of input radiance.

Temperature (°C)	Radiance (W cm^{-2} μ^{-1})
10	6.03E-05
15	7.44E-05
20	9.13E-05
25	1.11E-04
30	1.35E-04
35	1.62E-04
40	1.94E-04
45	2.31E-04

Table 2: Conversion between temperature and radiance for CE camera
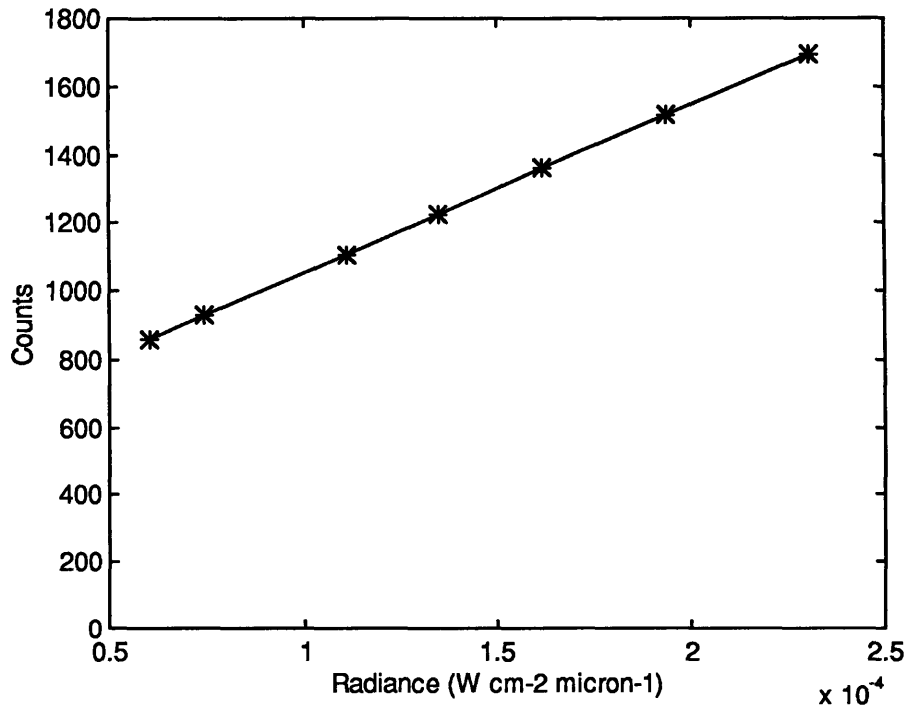
Figure 3-4: Relationship between blackbody radiance and sensor counts

3.2.2 Nonuniformity as a Function of Scene Radiance

While the previous graph shows the average relationship between array input and output, it gives no sense of the array nonuniformity. The presence of multiplicative terms in the nonuniformity will result in nonuniformity that is a function of scene radiance. Figure 3-5 shows a measure of nonuniformity as a function of the blackbody temperature. The nonuniformity is measured as the standard deviation of the response over the array as a function of the temperature of the imaged blackbody. Using the information in Figure 3-3, we can map the count axis to a temperature axis. For example, a standard deviation of 80 counts corresponds to a standard deviation across the array of approximately 3°C.
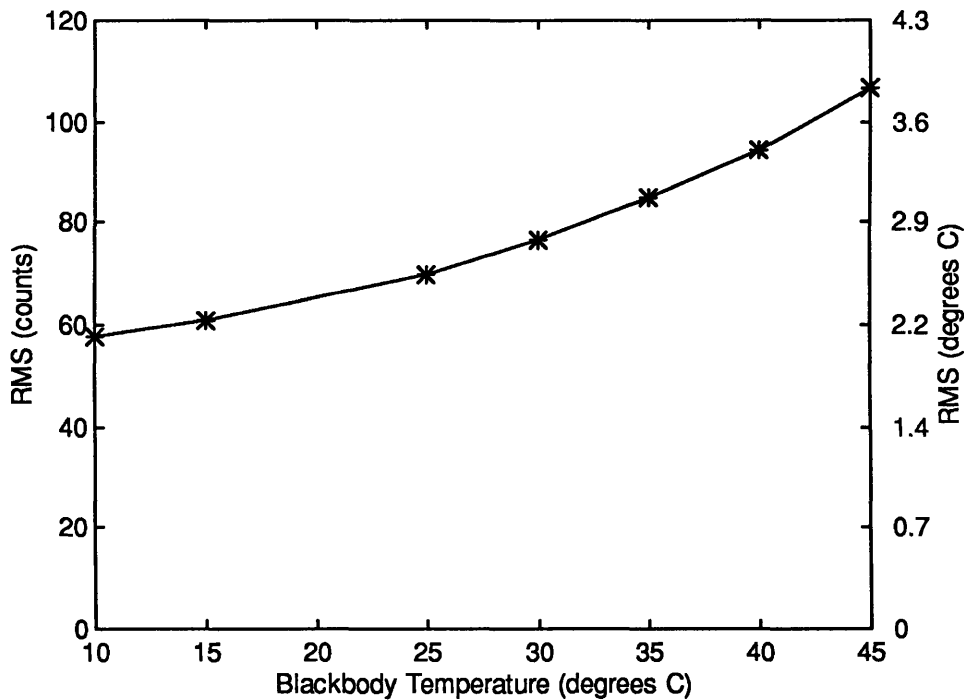
Figure 3-5: Standard deviation of InSb array response as a function of blackbody temperature

3.3 Spatial Characteristics of Nonuniformity

The spatial characteristics of interest are not only nonuniformity magnitude, but the spatial frequency of the nonuniformity. If the nonuniformity has a low spatial correlation (high spatial frequency) then it has many of the same characteristics as a potential unresolved target. If the nonuniformity were to have a low spatial frequency, that is, if the nonuniformity varied slowly across the array, then it would very likely pose little or no problem to subsequent target detection, as scenes are typically processed with a high-pass filter prior to detection. In Chapter 2, we saw an example of an uncorrected infrared image, which appeared to have low spatial correlation. In this section we will quantify those results.

The graphs in Figure 3-6 though Figure 3-9 plot the horizontal and vertical spatial autocorrelation of an image of a blackbody source. Since the background image is constant, any variation in the image is due to nonuniformity. By making an estimate of the correlation between pixels in the array, we are estimating the correlation of the nonuniformity. The figures show that the correlation falls off significantly for a difference of one pixel, which indicates the presence of high spatial frequencies in the sensor nonuniformity.
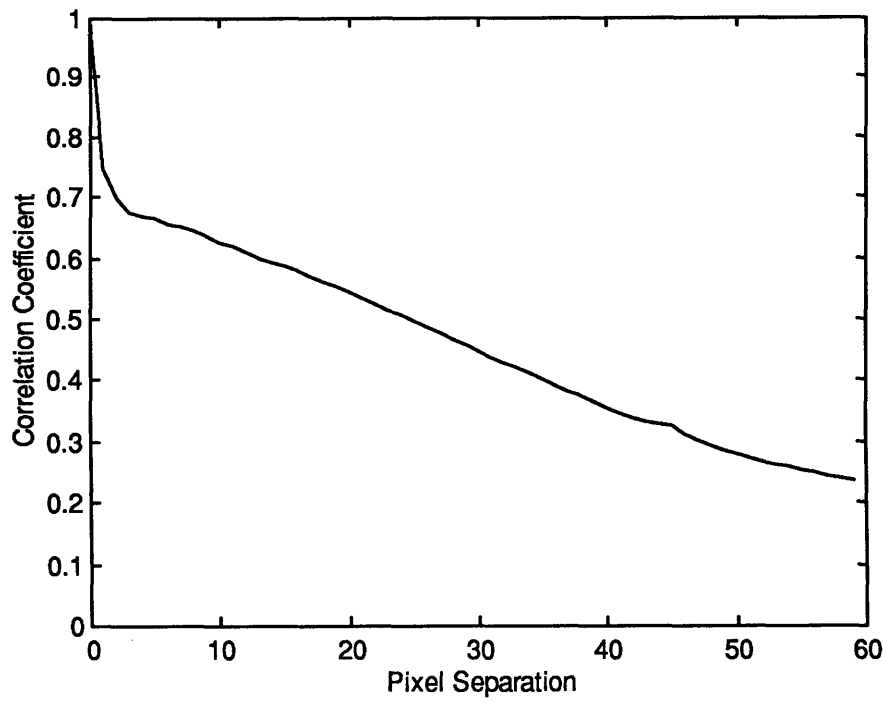
Figure 3-6: Horizontal spatial correlation of nonuniformity
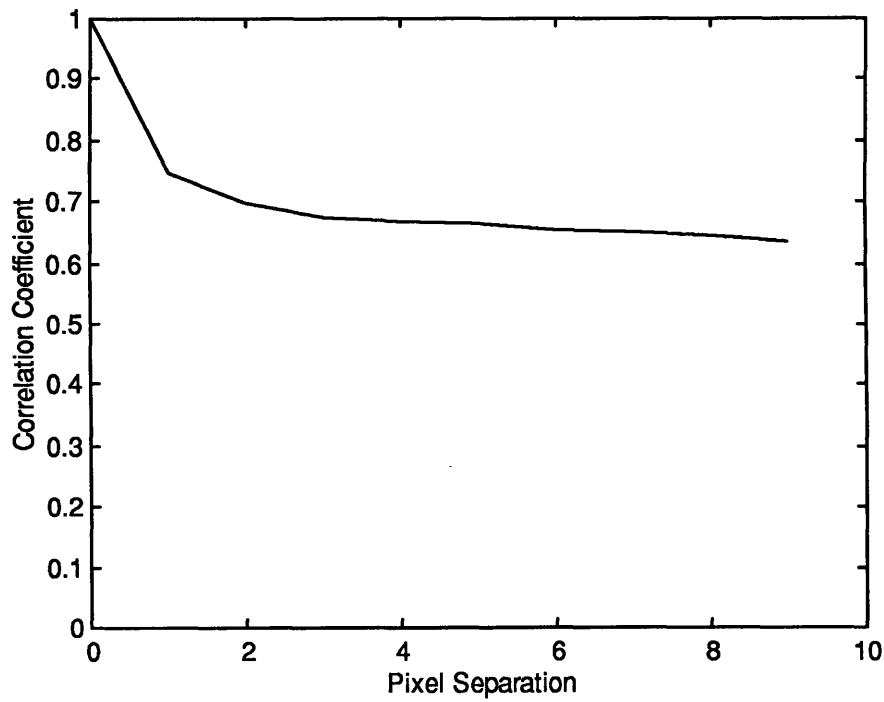
Figure 3-7: Horizontal spatial correlation of nonuniformity
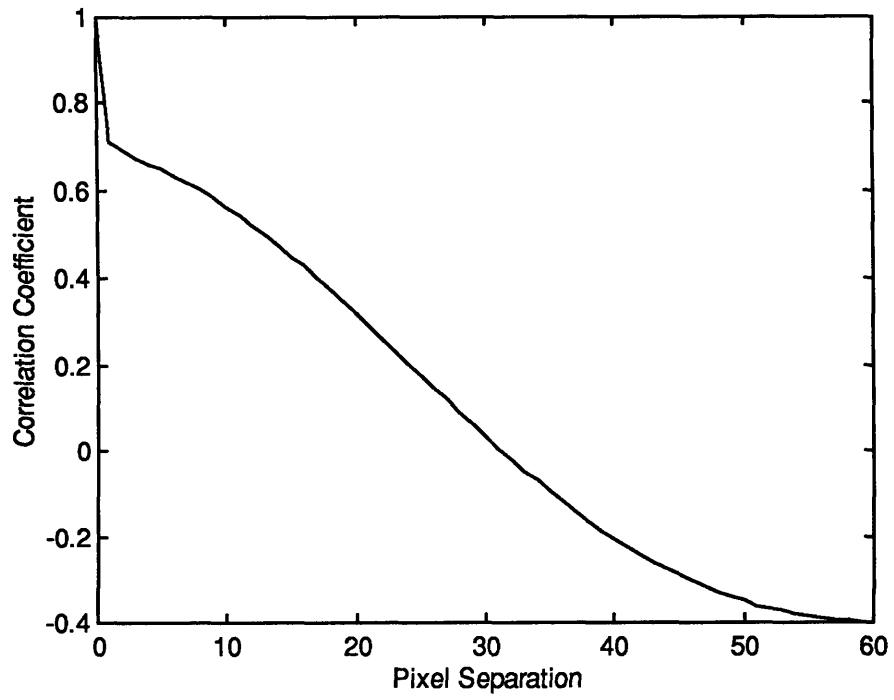
Figure 3-8: Vertical spatial correlation of nonuniformity
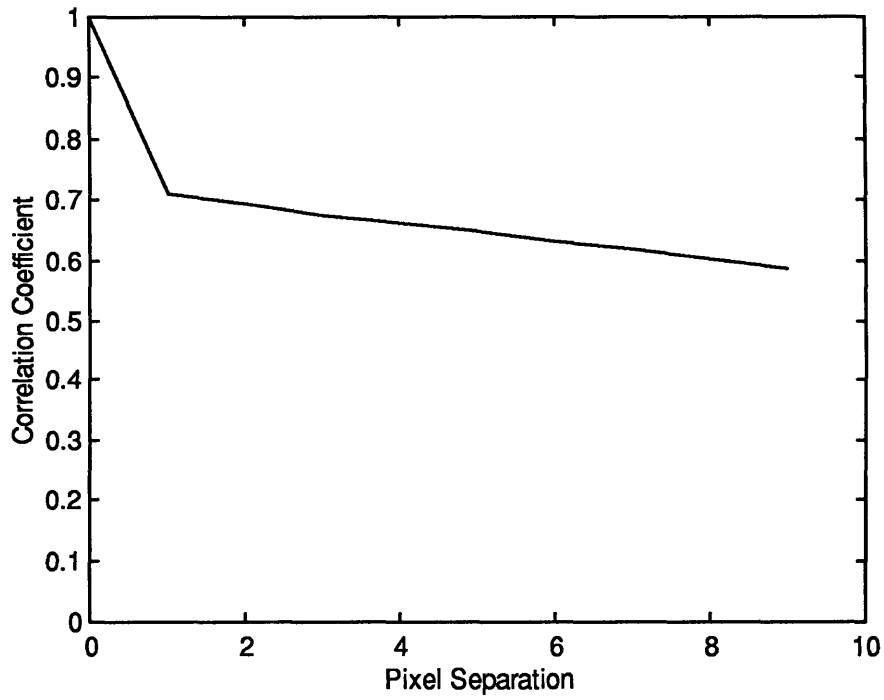
Figure 3-9: Vertical spatial correlation of nonuniformity

3.4 Temporal Characteristics of Nonuniformity

If the nonuniformity were constant in time, then we could perform compensation just once, and we would expect the performance of the compensation algorithm to remain high. However, drift in FPA parameters and differences in operating conditions cause a drift in the nonuniformity. This requires that compensation be performed periodically, in order to keep the nonuniformity compensation as accurate as possible.

To get an indication of the magnitude of the drift, Figure 3-10 shows the response of an InSb array to a 25°C blackbody over a period of 6 hours. The units of counts are not very revealing about the magnitude of the nonuniformity. However, the temperature scale on the right axis, which was calculated from the data in Figure 3-3, indicates that over the viewing period the array response would drift almost 0.5°C. That is, a blackbody of 25°C would appear to warm up to almost 25.5°C after a number of hours. These data indicate that the mapping between sensor counts and temperature changes with time, that is, that recalibration is necessary to get an accurate measurement of temperature. However, it is not clear from the mean response of the array how the nonuniformity changes with time.
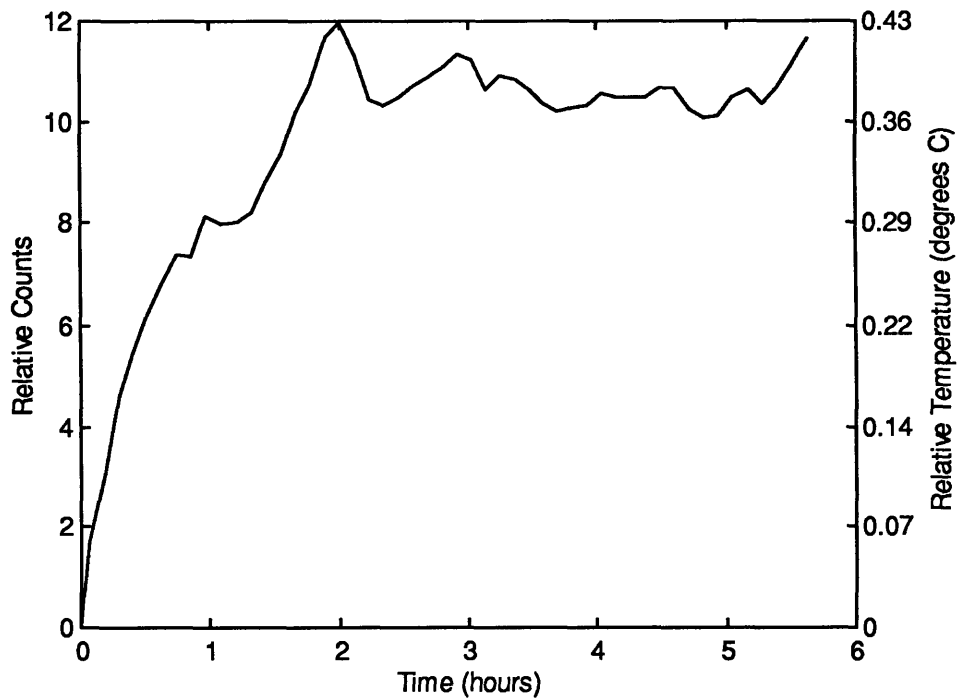
Figure 3-10: Relative drift of mean blackbody response of InSb array (the initial mean value of 1065.6 counts was subtracted from all mean values)

The standard deviation of the response of the array to a blackbody is a measure of the magnitude of the nonuniformity. In addition to the appearance of temperature drift over time, the magnitude of nonuniformity appears to increase over a period of time. Figure 3-11 shows the drift in the standard deviation of the response to the 25°C blackbody. The drift in the standard deviation of the FPA response, although very small over the 6 hour time period, indicates that the performance of any nonadaptive nonuniformity algorithm will degrade with time.
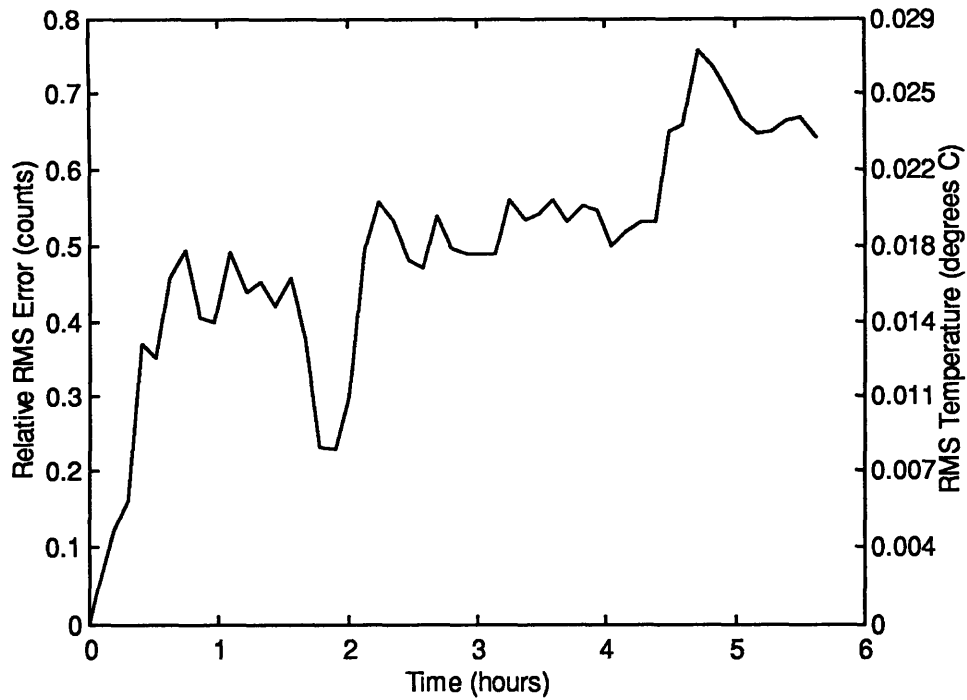
Figure 3-11: Drift of standard deviation of blackbody response of InSb array (the initial standard deviation of 73.7 counts was subtracted from all standard deviation values)

3.5 Summary

The measurements and analysis of blackbody data in this chapter illustrate the important features of nonuniformity. The high spatial frequency and relatively large magnitude prove the need to compensate for nonuniformity prior to target detection. The drift in array response indicates that successful compensation algorithms will need to be adaptive. Finally, the relative importance of gain and offset correction needs to be examined when evaluating compensation algorithms.

4 Source-Based Nonuniformity Compensation

In this chapter source-based nonuniformity compensation algorithms will be examined. This evaluation will provide a basis of comparison for the scene-based nonuniformity compensation algorithms addressed in Chapter 5. After a discussion of implementation, the performance of these algorithms will be presented using data from the CE camera used in Chapter 3.

In source-based compensation techniques, one or more uniform sources are used to estimate the nonuniformity compensation coefficients. The number of compensation coefficients depends on the number of temperatures imaged, as illustrated in Figure 4-1. If we take a blackbody measurement at one temperature, we can obtain an offset correction term for each detector element in the array. If we take a second temperature measurement, then we can also compensate for gain variations in each pixel. Any additional temperature measurements can be used to compensate for higher order terms or to do piecewise-linear compensation between adjacent temperature values. The specific calculations of the coefficients will be covered in the performance examples.

In addition to using blackbody measurements to perform nonuniformity compensation, these blackbody measurements can be used to perform calibration. One advantage of source-based techniques is that they can be used to calibrate the sensor as calibrated blackbody frames are measured.
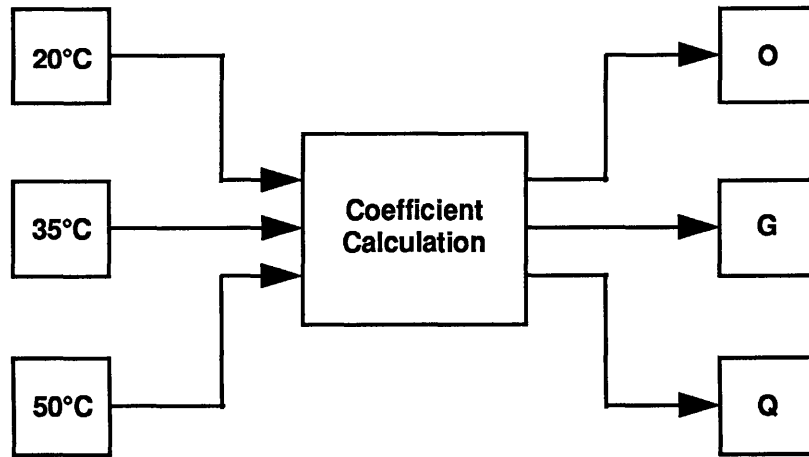
Figure 4-1: Compensation block diagram

4.1 Implementation Issues

The two-or-more-point nonuniformity compensation techniques are not computationally complicated to implement; however, taking the calibration frames presents various problems. Inserting the blackbody into the field of view of the sensor requires additional hardware and optics; in some systems, the array is mechanically rotated in its housing to view the blackbody reference which is located behind the array. Another potential implementation problem is that the blackbody temperature must be accurately controlled, which requires a precision cooling and heating system.

In addition to hardware requirements for source-based nonuniformity compensation, measurements of the uniform calibrated source must be obtained. The time required to make these measurements is time that cannot be spent imaging scene information.

Finally, the change in nonuniformity with time requires that compensation coefficients be recalculated periodically, based on the FPA characteristics. The time frame over which recalibration must occur depends on the performance requirements for the imaging system.

4.2 Performance

The performance of the source-based algorithms depends on the number of uniform temperature sources used. It is expected that the more temperatures that are used in the compensation, the better the performance, assuming that the temperatures of the blackbodies span the range of expected scene temperatures. However, there is a tradeoff between the accuracy of the compensation and the amount of time and storage that is associated with calibrating at multiple temperatures. Most applications use two-point compensation. If more than two temperature points are used, it is generally for the purpose of performing piecewise-linear compensation.

The experimental data used to evaluate the performance of the one-point and two-point nonuniformity compensation (NUC) techniques are the blackbody data obtained from measurements using the CE camera to image blackbodies of varying temperatures.

There are two types of noise in the sensor, nonuniformity, or fixed pattern noise, and temporal noise, which consists of photon noise and additive readout noise. The photon noise is a function of the exposure and will vary from frame to frame. As exposure levels increase, the photon noise becomes less significant, since it grows as the square root of the exposure. To minimize the effects of temporal noise in the compensation, multiple

frames of data are averaged together before calculating correction coefficients. In the measurements in this section, the coefficients are applied to averaged frames, rather than individual frames. This reduces temporal noise variations that will contribute to the compensation error. The temporal noise is investigated as a separate issue.

4.2.1 One-Point Compensation

In one-point compensation, data at one temperature are required and only an offset correction term is calculated. The calculation for the offset correction term for each pixel, $o(i, j)$ is as follows:

$$\mu_L = \frac{1}{N} \sum_i \sum_j c_L(i, j) \, ,$$
$$o(i, j) = \mu_L - x(i, j)$$

where c_L is the low temperature calibration frame. The offset term will correct each pixel in the calibration frame to be the mean value of the array response, μ_L.

In the following example, a 25°C blackbody was used as the compensation temperature. To minimize the effects of temporal noise, the offset coefficients were calculated from a 200-frame average. The derived offset compensation coefficients were then added to the 200 frame-averaged images of the blackbody sources over a range of temperatures, thereby isolating the fixed pattern noise from the temporal noise. Since we are imaging a uniform source, the standard deviation of the compensated images is the residual compensation error.

Figure 4-2 illustrates the standard deviation of the corrected images. At 25°C, the compensation temperature, the error is zero. This was forced to be the case because this

40

compensation technique calculates the offsets by eliminating the variance at the compensation temperature. However, the error increases the further the blackbody temperature is from the compensation temperature. The left axis is the standard deviation in sensor counts, while the right axis indicates the equivalent standard deviation in temperature (using the data from Figure 3-3).
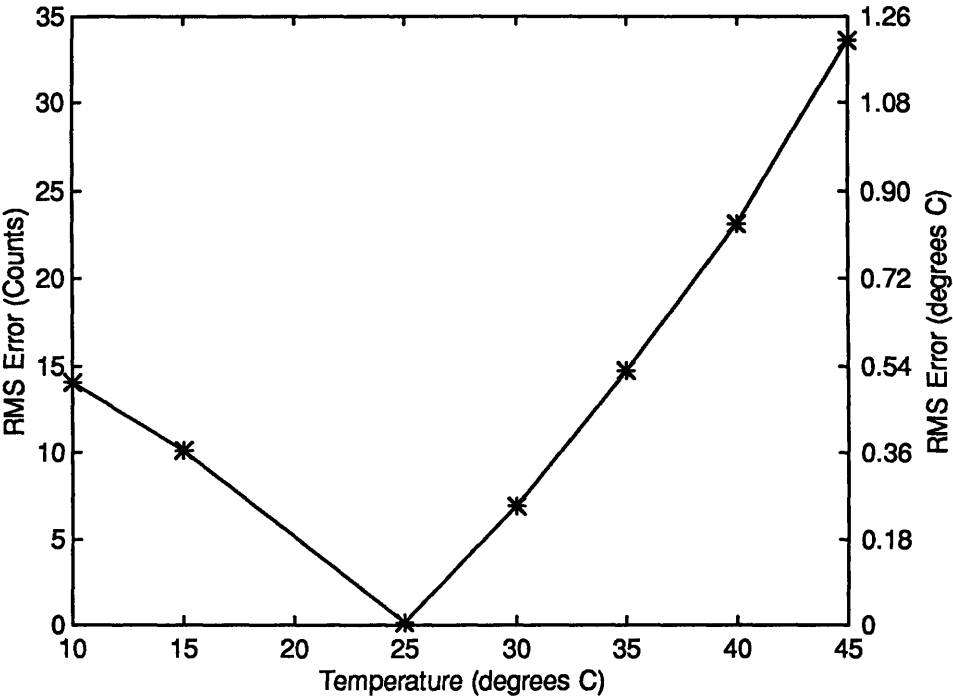
Figure 4-2: One-point NUC using 25°C as calibration temperature

This implies that the offset correction is optimized for images whose scene temperature is close to that of the blackbody used for compensation. Figure 4-3 plots the standard deviation of the original images as well as the error after one-point

compensation. It is apparent that the error after compensation is significantly less than original nonuniformity, even at temperatures away from the offset temperature.
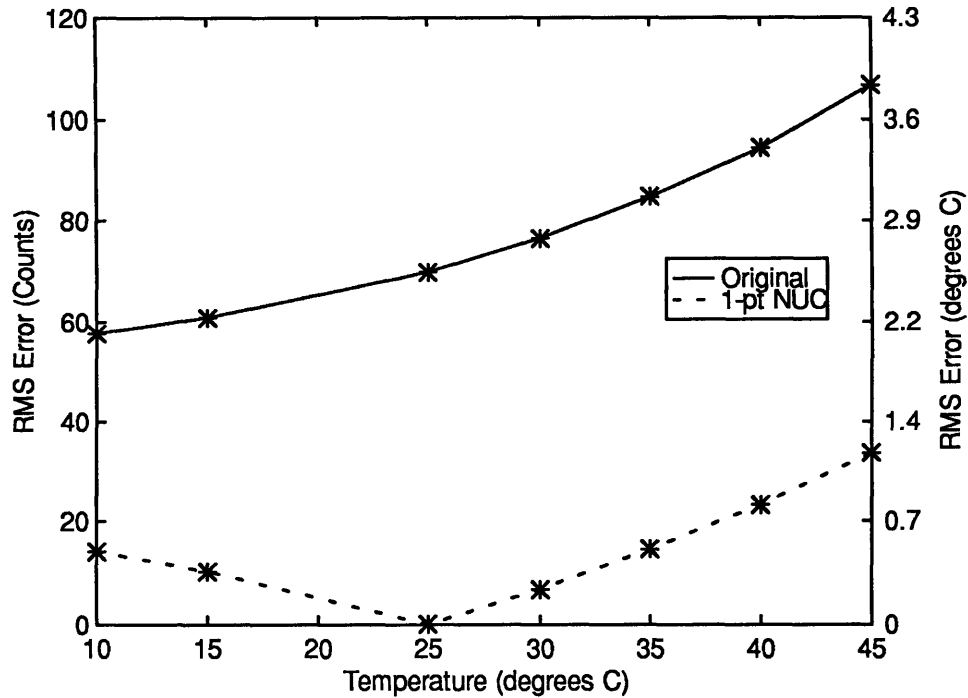
Figure 4-3: Comparison of original array nonuniformity and error after one-point NUC

4.2.2 Two-Point Compensation

In two-point compensation, data from two temperatures are required to calculate offset and gain coefficients. Since the result of the one-point compensation indicated that the best performance occurred close to the compensation temperature, the compensation temperatures should span the expected range of scene temperatures.

The offset and gain coefficients, o(i, j) and g(i, j) can be calculated as follows:

$$\mu_L = \frac{1}{N} \sum_i \sum_j c_L(i, j)$$

$$\mu_H = \frac{1}{N} \sum_i \sum_j c_H(i, j)$$

$$g(i, j) = \frac{\mu_H - \mu_L}{c_H(i, j) - c_L(i, j)}$$

$$o(i, j) = \mu_L - c_L(i, j) \frac{\mu_H - \mu_L}{c_H(i, j) - c_L(i, j)},$$

where c_L and c_H are the low and high temperature calibration frames. As is the case with the one-point compensation, the gain and offset coefficients correct each pixel in the compensation frames to their respective means, μ_L and μ_H.

In the next example, the compensation temperatures were 25°C and 40°C. Again, 200-frame averages were constructed in order to calculate the offset and gain coefficients. These coefficients were applied to the same set of data as the one-point compensation algorithm. The standard deviation of the corrected images is a measure of the residual compensation error.

Figure 4-4 is the graph of the compensation error as a function of the blackbody temperature. As with the one-point compensation, the minimum error is achieved at the compensation points.

,
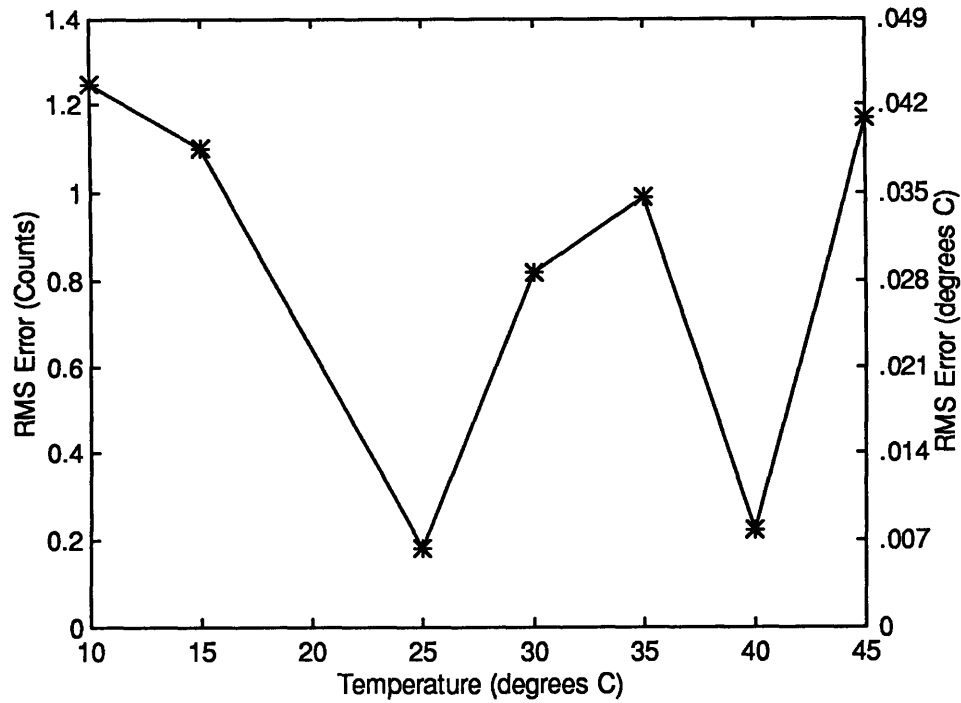
Figure 4-4: Two-point NUC using 25°C and 40°C as calibration temperatures

The performance of the two-point nonuniformity compensation algorithm was considerably better than that of the one-point algorithm. Figure 4-5 compares the performance of the two-point technique with the one-point technique and the original image nonuniformity.
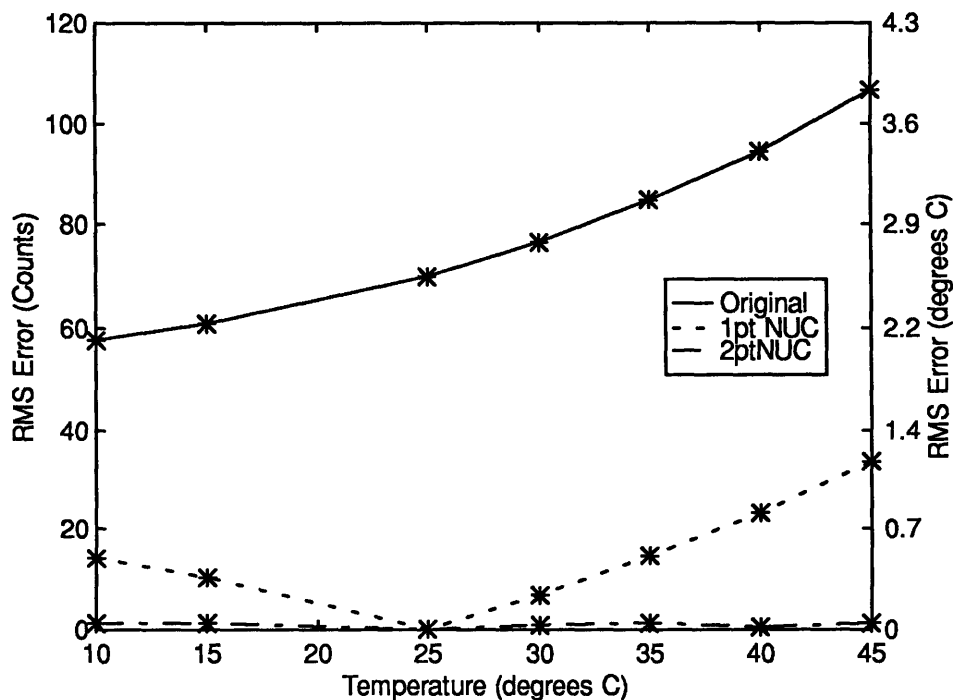
Figure 4-5: Comparison of original nonuniformity with one-point and two-point NUC

4.2.3 Temporal Noise Consideration

In the previous treatment of one-point and two-point nonuniformity compensation, the techniques were applied to averaged frames of data, in order to lessen the effects of temporal noise. To estimate the effects of the temporal noise on the compensated image, we can apply the correction coefficients to individual frames of data, rather than the 200-frame averages as in the previous sections. Figure 4-6 illustrates the variation in the individual frames of data after one-point correction. These variations are significantly less then compensation error that is present in Figure 4-2, and therefore are not the dominant source of error in the system, except at or very near the calibration temperature.

45
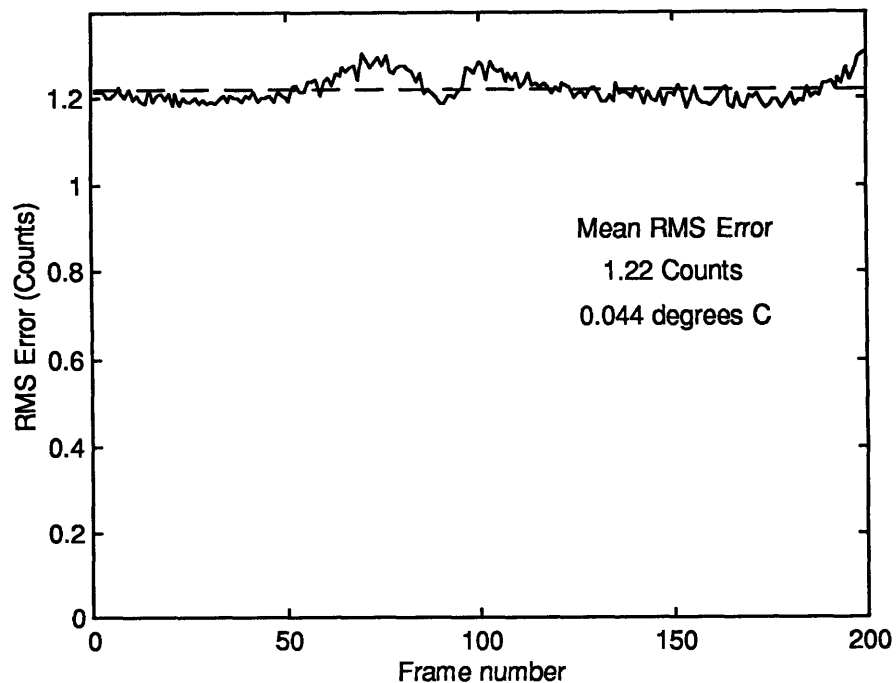
Figure 4-6: Standard deviation of single frames after applying offset correction to 200 consecutive frames (frame rate = 51.44 Hz)

To observe the magnitude of the temporal noise, we examine the response of a single pixel after compensation. The average response of the individual pixel over the 200 frames is identical to the average corrected value over the array, and the fluctuations, shown in Figure 4-7, are a result of the temporal noise. The variation in response is approximately 1.3 counts (0.046°C). Comparing this value with the one-point and two-point compensation performance in Figure 4-2 and Figure 4-4, it is clear that this temporal noise dominates for the entire range of temperatures in the two-point nonuniformity

compensation and at the calibration temperature in the case of one-point nonuniformity compensation.
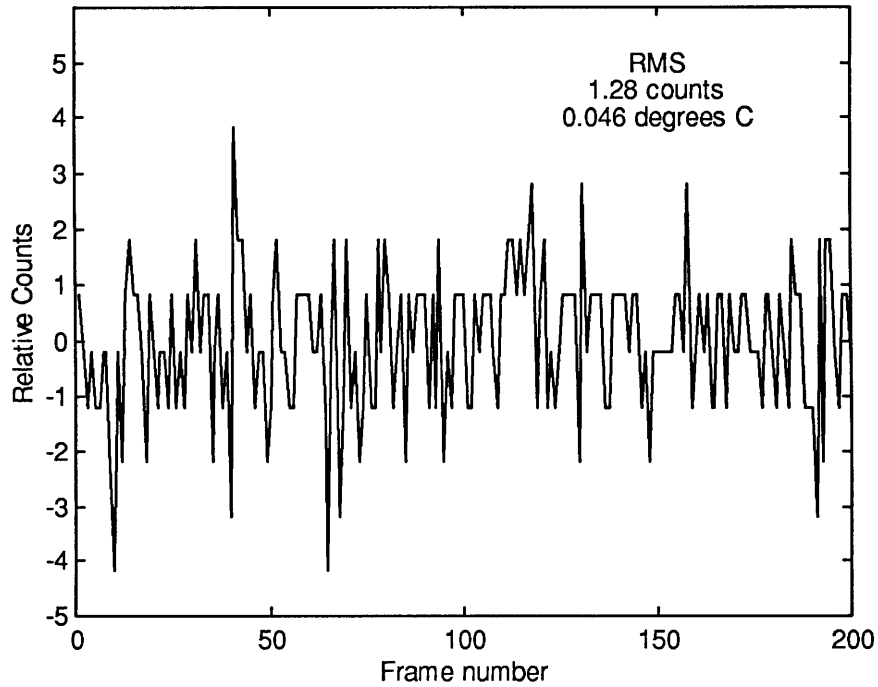
Figure 4-7: Temporal variation of one pixel after offset compensation (minus mean pixel value of 1223.2 counts)

4.2.4 Investigation of Gain and Offset Terms

Once we have the gain and offset terms for a calibration frame, we can return to the issue of the relative importance of the gain and the offset portions of the nonuniformity. Histograms of the offset and gain coefficients for the previous two-point nonuniformity compensation algorithm are presented in Figure 4-8 and Figure 4-9 respectively. From these coefficients we can determine the effects of the gain and offset

47

terms of the nonuniformity. The contribution of the offset term is its standard deviation, 31.3 counts. The contribution of the gain term at each temperature is the standard deviation of the gain coefficients, 0.047 counts, multiplied by the output in counts at that temperature. For the 25°C blackbody, the average output was 1107 counts, which means the standard deviation of the gain component was 52.0 counts. This indicates that compensation for the gain term is indeed important for removing nonuniformity.
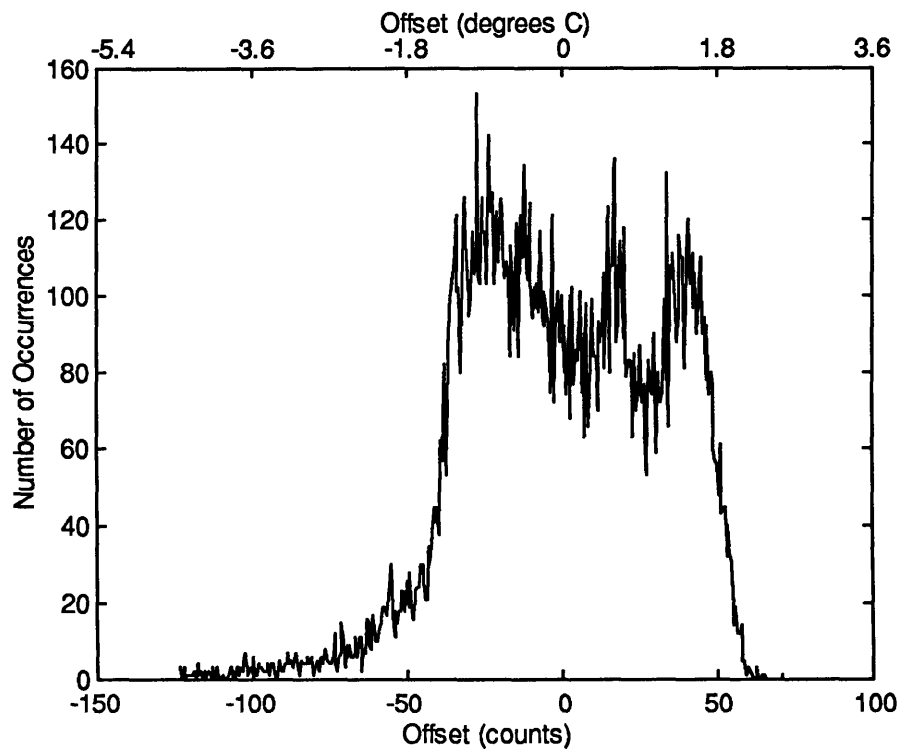
Figure 4-8: Histogram of Offset Coefficients in 2pt NUC
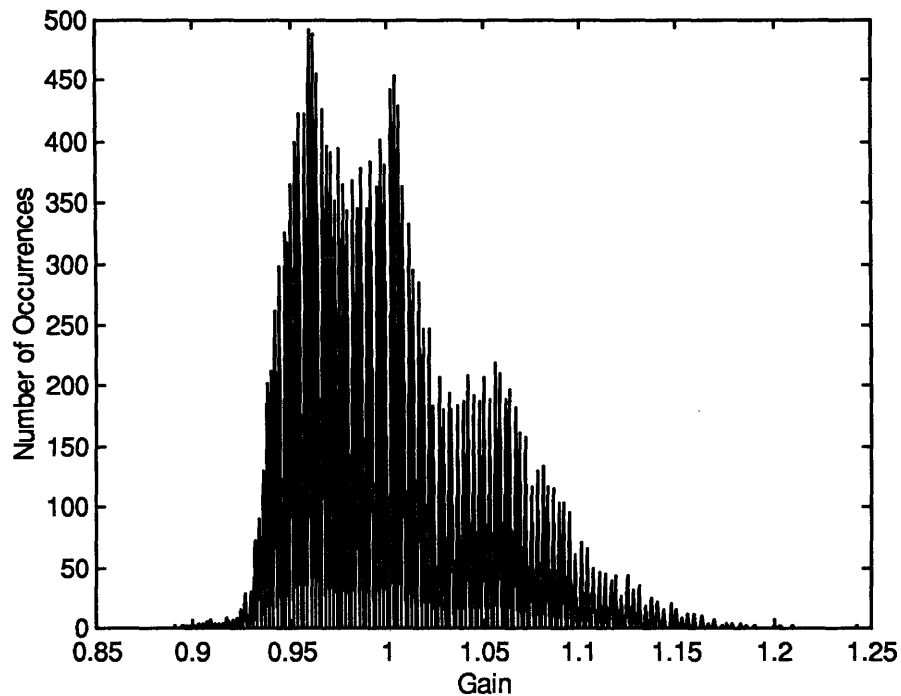
Figure 4-9: Histogram of Gain Coefficients in 2pt NUC

From these coefficients, we can make an estimate of the nonuniformity in the array. In the previous chapter we assumed that the multiplicative and additive components dominate the nonuniformity. These components are calculated from the gain and offset coefficients as follows, where a is the additive component and b is the multiplicative component,

$$b(t) = \frac{1}{g(t)}$$

$$a(t) = -\frac{o(t)}{g(t)}.$$

This relationship will be used in the next chapter, to create nonuniformities in data for the purposes of testing scene-based algorithm performance.

4.3 Summary

Source-based techniques work very well near the compensation temperatures. The resulting compensation error, across the wide range of temperatures was far lower than the original scene nonuniformity. Two-point compensation techniques outperform the one-point techniques across the 10°C - 45°C temperature range, on average, by a factor of 18 to 1.

5 Scene-Based Nonuniformity Compensation

In this chapter the characteristics of scene-based nonuniformity compensation algorithms are examined. The performance of one of these algorithms will be evaluated and compared to the source-based compensation techniques using both blackbody measurements and terrain scene data collected using an airborne IR sensor. A method for determining the parameters for optimal performance, as a function of the temporal correlation of the data, is developed and tested.

Scene-based nonuniformity compensation techniques use scene data, instead of blackbody calibration data, to estimate and compensate for array nonuniformities. One advantage of these techniques is that they are adaptive and can potentially compensate for drift in FPA response. Another advantage of scene-based techniques is that they do not require blackbody data, which can simplify the imaging system.

There are, however, potential drawbacks to scene-based techniques. First, the technique computes estimates of the compensation parameters and may thus result in additional errors relative to source-based techniques. Also, the scene-based techniques are only compensation techniques, they do not provide the absolute temperature reference that is found with source-based methods. Finally, there is an added computational cost relative to source-based techniques.

The simplest implementation of a scene-based algorithm constructs an estimate of the offset nonuniformity using some form of weighted averaging over diverse scenes. This is similar to the one-point source-based compensation. However, as illustrated in Chapter

4, the offset correction only performs well at or near the calibration temperature. The effect of the scene-based algorithms is to perform the one-point compensation, but with the adaptive features it is similar to performing one-point compensation with a blackbody source whose temperature is always the average scene temperature. While this is an advantage, the performance will depend on the characteristics of the background scene, as will be discussed later in the chapter.

5.1 Implementation Issues

One implementation is to use a temporal high-pass filter to correct each pixel $x(i,j,n)$ individually, where n is the frame number and (i,j) denotes the location of the pixel in the array. In this case, an average of the previous pixel values, $f(i,j,n)$, is constructed, giving more weight to the more recent pixels, and then subtracted from $x(i,j,n)$ to yield the compensated pixel value, $y(i,j,n)$. This can be accomplished with the use of a recursively computable low-pass filter, as follows,

$$y(i,j,n) = x(i,j,n) - f(i,j,n)$$
$$f(i,j,n) = \frac{1}{m}x(i,j,n) + \frac{m-1}{m}f(i,j,n-1),$$

where m is used to shape the impulse response of the temporal filter. The optimal value for m depends on the characteristics of the background scene

Since each pixel is corrected independently of the other pixels in the array, there is a constraint on the background scene. The assumption is that the computed offset, which is an estimate of the nonuniformity, is the sum of the average value of the nonuniformity and the average value of the scene at that pixel. In order to make an accurate estimate of

the nonuniformity, we need to guarantee that the average scene radiance that is imaged by each pixel is the same across the array. If this is not the case, variations in the scene from pixel to pixel may not be preserved. This is a trivial constraint when applying the scene-based techniques to blackbody data, since the scene radiance is, by definition, constant across the array. However, this is an issue when we apply the filter to scenes that have spatial variations.

5.2 Performance

The initial performance measures of this scene-based techniques are made by applying the temporal high-pass filter to the blackbody data from the CE camera. The performance can be compared directly to that of the source-based offset compensation technique. This comparison is not a complete evaluation of the technique since scene characteristics will affect the performance of the algorithm, but it provides a starting point for the analysis.

After applying the temporal high-pass filter to blackbody data, we will examine the performance on synthesized images of a given temporal correlation and imposed nonuniformity. These images were created by segmenting a large single image obtained from the Infrared Measurements Sensor (IRMS). The IRMS is a dual waveband (MWIR and LWIR) scanning system, which can image 20° in azimuth and 2.25° in elevation, and has an instantaneous field of view (IFOV) of 100 μrad. A metric for determining the optimal value of m, based on the temporal correlation of the scenes, is developed using these controlled scenes.

After evaluating the performance on the simulated data, the algorithms are applied to scene data obtained from the Skyball airborne IR sensor. The Skyball system uses 128x128 HgCdTe FPAs for the MWIR (3.4 - 4.9 μm) and LWIR (7.6 - 9.4 μm) wavebands; in this thesis we use the MWIR waveband data. The system has a 1.74°x1.74° FOV and an IFOV of 238 μrad. There are calibration frames preceding and/or following the scenes, which allow for a comparison between source-based and scene-based techniques.

5.2.1 Offset Comparison with Source-Based Techniques

We have already examined offset correction for one-point source-based compensation. To compare the performance of the scene-based temporal high-pass filter with that of the one-point compensation, we apply the algorithms to the CE camera images of a 25°C blackbody, as used in the temporal noise measurements in Chapter 4. Since the scene is constant, we can examine the steady state performance of the temporal high-pass filter for various values of the filter parameter m.

The results of applying the temporal high-pass filter are shown in Figure 5-1. The residual error after compensation is illustrated for three different values of m. As evident in the graph, the number of frames it takes for the algorithm to reach steady state performance is proportional to m. As the value of m increases, more frames of data are required for the filter to adapt to sudden changes in the scene.

Figure 5-1: Performance of scene-based temporal high-pass filter applied to 200 frames of blackbody data at 25°C

To get a better indication of the performance of the temporal high-pass filter, Figure 5-2 shows the steady state performance (frames 100-200) for the three values of m used in Figure 5-1. The general behavior is similar for the three values of m. However, the lower the value of m, the lower the average steady state error. This is a result of the filter implementation; for low values of m, more of the current frame is used in the estimate of the nonuniformity, therefore more of the variations in an individual frame will be removed. This will have an impact on target detection, since targets may be suppressed along with the background.
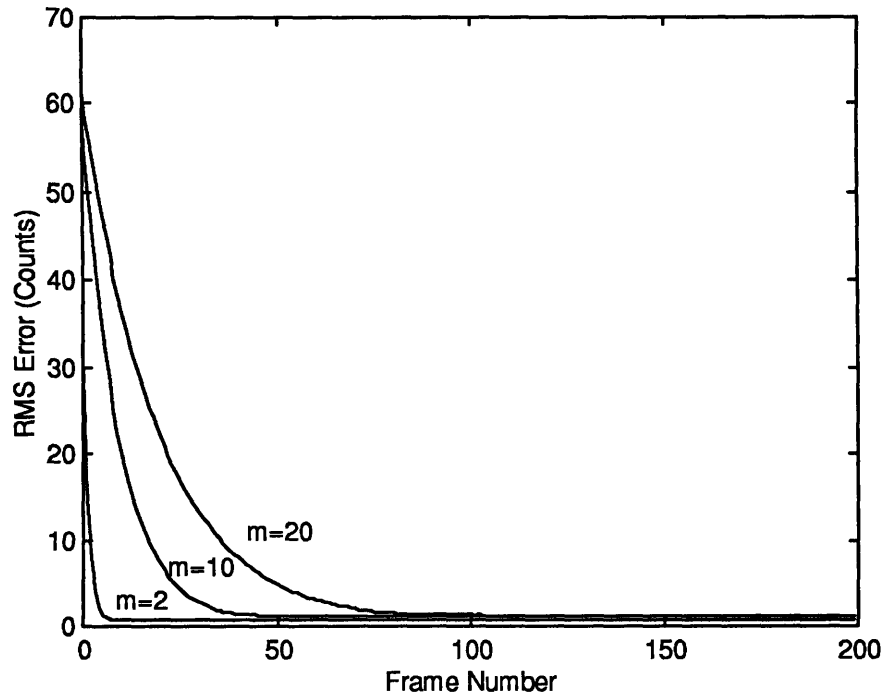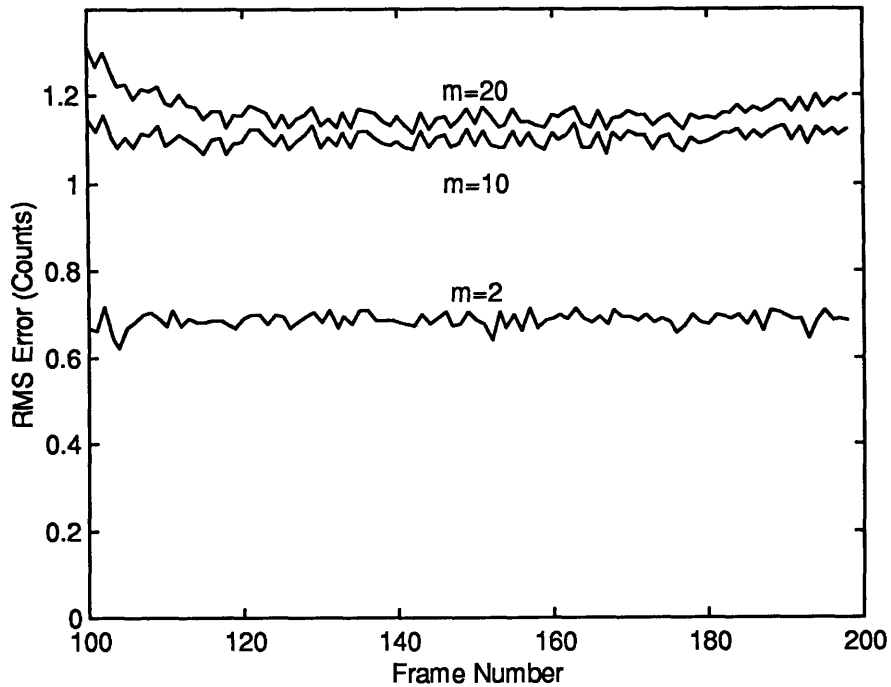
Figure 5-2: Performance of scene-based temporal high-pass filter applied to 200 frames of blackbody data at 25°C

In addition to comparing the temporal high-pass filter for different values of m, we would like to examine the performance relative to the performance of the one-point compensation discussed in Chapter 4. In Figure 5-3, the results of the temporal high-pass filter (for m=5) are compared to the results after one-point compensation. The offset for the one-point compensation is derived from an average of the 200 frames and then applied to each of the frames individually, as in Figure 4-6. The one-point compensation performance provided a measurement of the temporal noise limited performance. In the case of the temporal high-pass filter, the residual compensation error is lower than that obtained by the one-point compensation. This results from the use of a fraction of the current scene in the estimation of the nonuniformity, thus reducing some of the temporal

noise; in the case where we image actual scenes we will expect that this algorithm will also reduce clutter.

In order to verify that the higher residual error in the one-point compensation is not due to sensor drift, we also can apply an offset correction which simply subtracts a 5-frame local average from each input frame. This is indicated in Figure 5-3 by the dotted line. If there were significant drift, we would see that the local average would perform better than the offset calculated by averaging all 200 frames. Since this is not the case, background suppression, not drift in the sensor, is the reason for the decrease in residual error in the temporal high-pass filter.
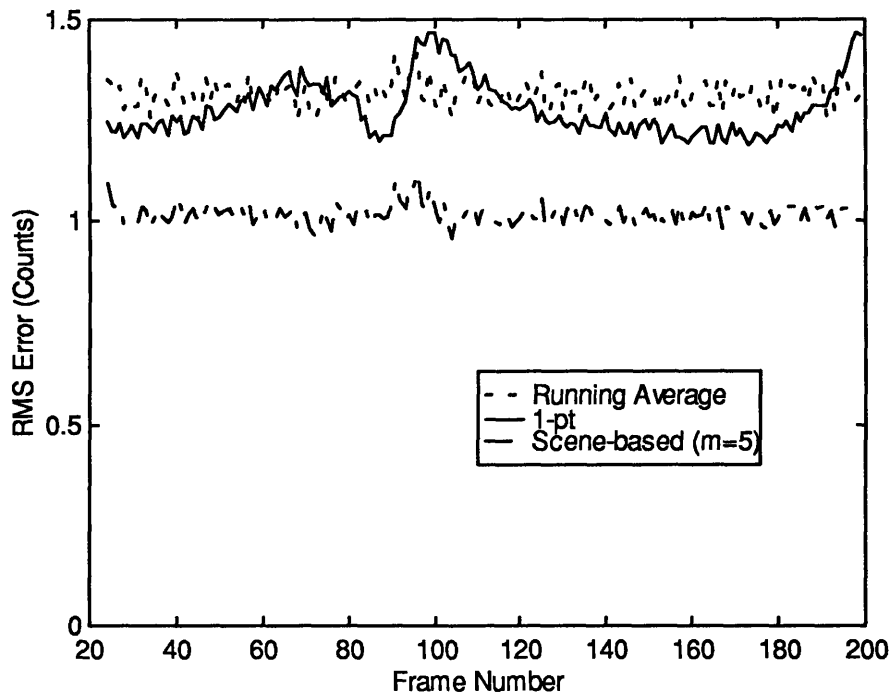
Figure 5-3: Comparison of temporal high-pass filter, running average, and one-point compensation applied to 200 frames from CE camera of blackbody at 25°C

5.2.2 Applying Algorithm to Synthesized Scene Data

By applying the scene-based algorithms to images of known background statistics and nonuniformity, a relationship between the temporal correlation of the scenes and the m factor in the temporal high-pass filter that yields optimal performance can be constructed. A rural scene recorded in Harvard, Massachusetts was used in this study; a portion of the image is shown in Figure 5-4. The mean temperature of the image is 9.1°C (1671.2 counts) and the standard deviation is 0.6°C (15.1 counts). This IRMS image was divided into a sequence of frames, where the apparent rate of motion of the frames is measured as the horizontal pixel separation between frames. By changing the apparent rate of motion of the scene, we can create scenes with different temporal correlation lengths; the temporal correlation function is simply a scaled version of the spatial correlation function. The rate term is the ratio of the spatial correlation length and the temporal correlation length,

$$rate = \frac{L_s}{L_t}.$$
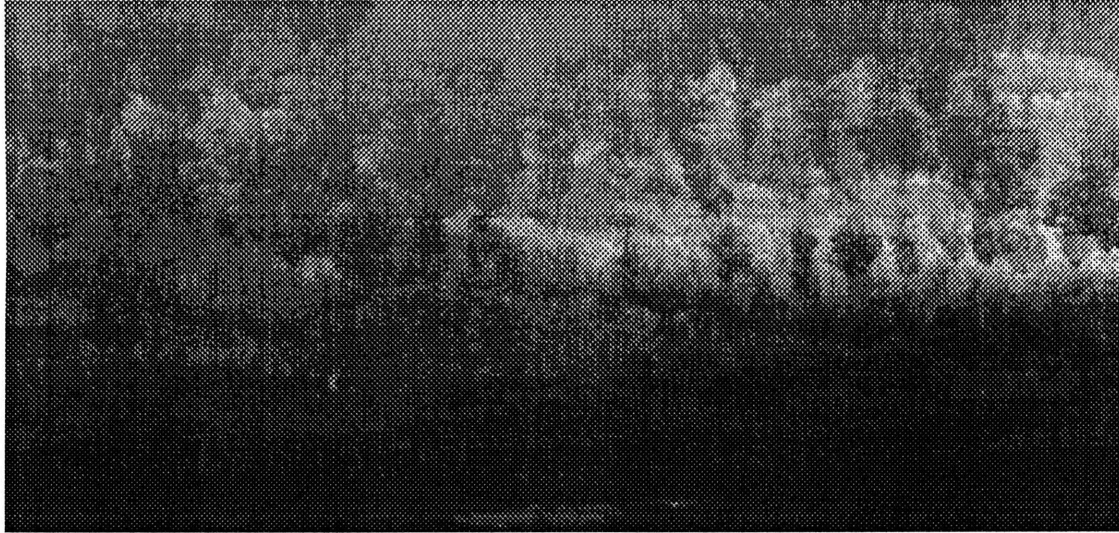
Figure 5-4: Section of IRMS image of Harvard, MA used to test temporal high-pass filter

Figure 5-5 shows the spatial correlation of the portion of the original IRMS image that was used to create the multiple frames of data. To estimate the spatial correlation length, we can fit the correlation data, R[n], to an exponential of the form,

$$R[n] = ae^{-n/L_s} + b,$$

where L_s is the spatial correlation length, and the a and b terms are scaling factors. As is apparent in Figure 5-5, the horizontal correlation of the image is high. The exponential fit to the correlation data is also shown in Figure 5-5 and the estimated correlation length is approximately 2 pixels.
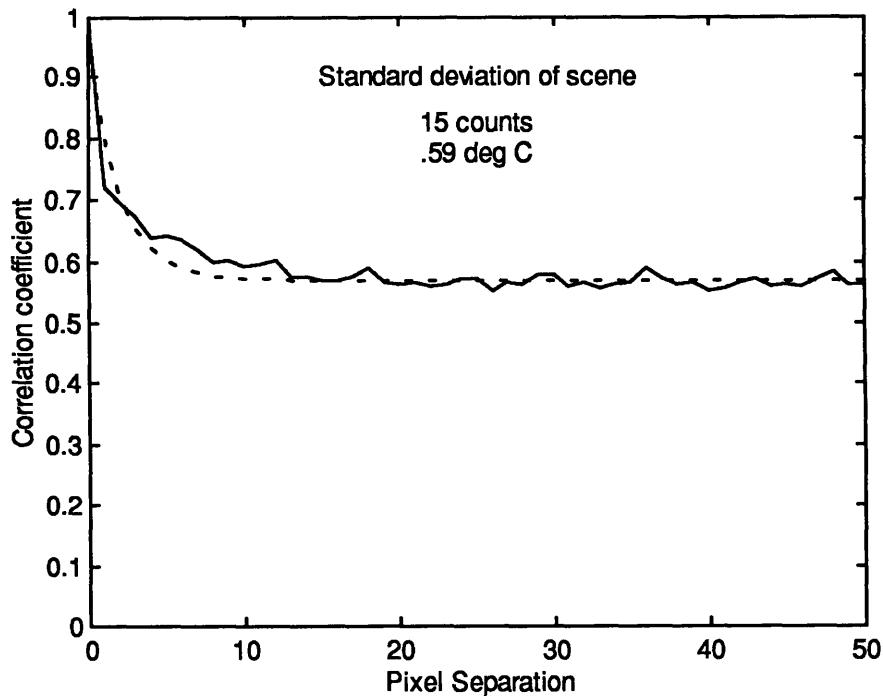
Figure 5-5: Horizontal spatial correlation of IRMS image (calculated in 100x100-pixel blocks).

The processing steps that were used to evaluate the performance of the temporal high-pass filter are shown in Figure 5-6. After segmenting the original images, nonuniformity is imposed. As discussed in Chapter 4, the gain and offset coefficients for a particular array can be used to estimate the multiplicative and additive factors that corrupted the original scene. The gains and offsets used in these cases were the coefficients that were calculated in Section 4.2.2 for the InSb array. These factors were applied to the sequence of images in order to create a nonuniformity; this nonuniformity would be compensated exactly by applying the gain and offset coefficients as previously calculated. It is important to note that there is no temporal drift in the imposed

nonuniformity. The advantage of imposing a known nonuniformity on the images is that the compensated images can be compared directly with the original images.
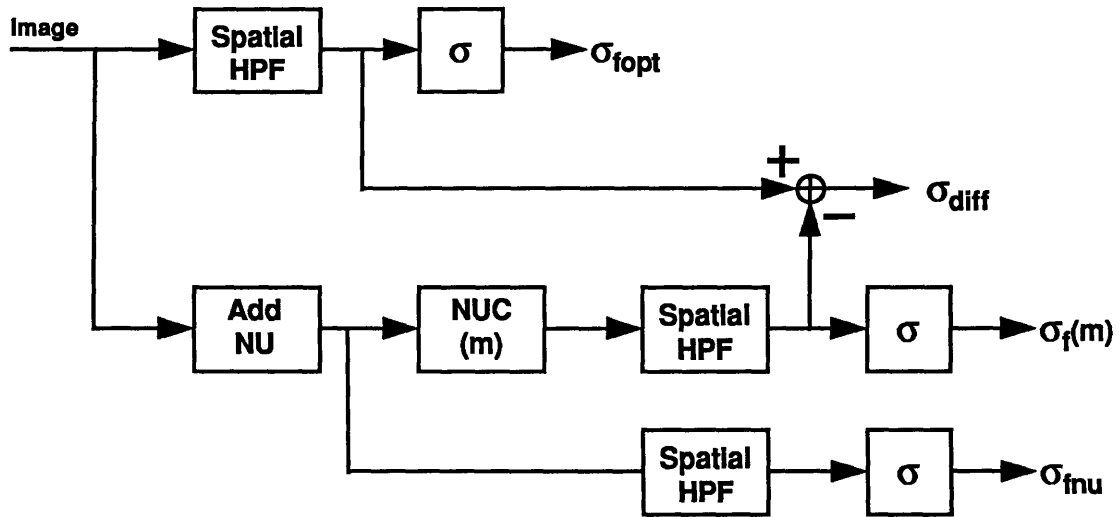
Figure 5-6: Block diagram of algorithm testing

A spatial high-pass filter (standard Laplacian filter) is applied to reduce scene clutter for subsequent detection of unresolved targets. The Laplacian filter employed in three places in Figure 5-6, can be represented as follows:

$$\begin{bmatrix} 0 & -\dfrac{1}{4} & 0 \\ -\dfrac{1}{4} & 1 & -\dfrac{1}{4} \\ 0 & -\dfrac{1}{4} & 0 \end{bmatrix}.$$

Any difference between the compensated frame and the original image (before the nonuniformity is imposed) after high-pass filtering is due to error in the nonuniformity compensation, and will be measured as the standard deviation of the differenced images, σ_{diff}.

The spatial high-pass filter eliminates most of the background clutter in the IRMS image. The effects of this can be seen in the autocorrelation of the filtered image, which is shown in Figure 5-7. The autocorrelation of the image, after filtering, drops very quickly to zero.
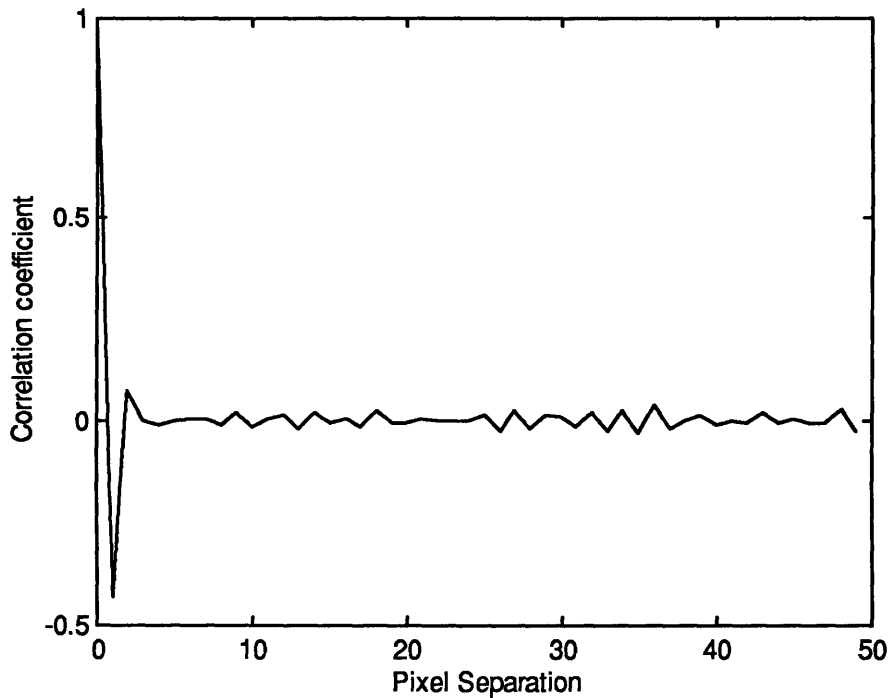
Figure 5-7: Autocorrelation of high-pass filtered IRMS image

The processing in Figure 5-6 was applied to data segmented at different rates, and for different values for m in the compensation filter. In Figure 5-8, the standard deviation of the difference between the high-pass filtered images, σ_{diff}, is shown as a function of the frame number and for three different values of m. The larger the value of m, the more frames are required to construct a good estimate of the nonuniformity. For the case where

m=2, the algorithm reaches the steady state value (σ_{diff} = 1.2) counts very quickly (less than 10 frames). For m=25, the steady state value of σ_{diff} is lower (0.36 counts), however, more frames are needed to achieve steady state performance. In the case of m=75, steady state performance has not been achieved in the 169 frames used in this sequence of images. The effect of large values of m is that when the scene changes rapidly, the algorithm is slower to adapt and reach steady state performance. Small values of m may have a faster response to changes, but as evidenced in Figure 5-8, this results in decreased performance in the steady state.
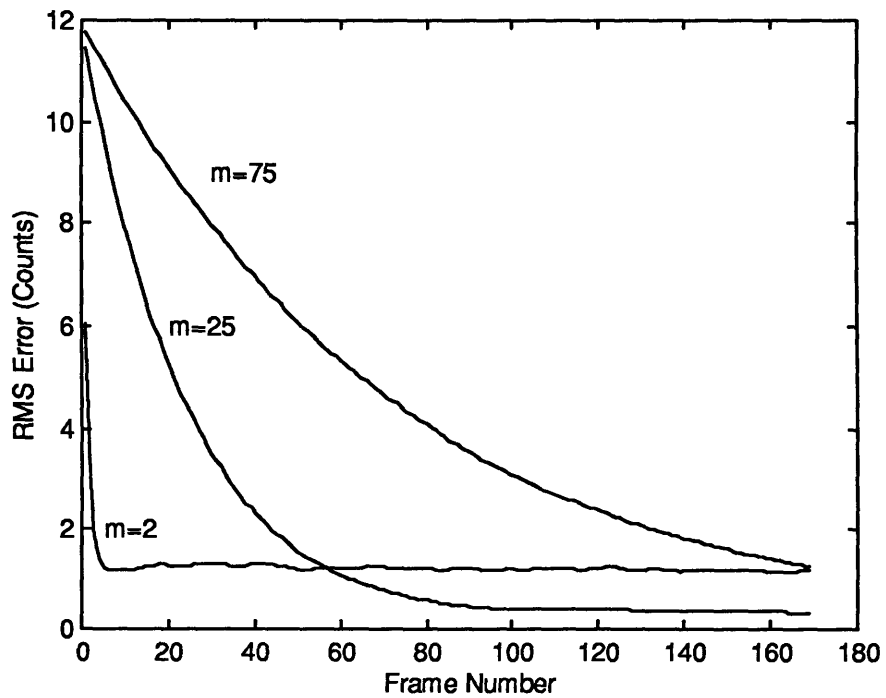
Figure 5-8: Performance of temporal high-pass filter (rate=20)

By constructing these curves for a number of different rates, we can find the value

of σ_{diff} in the steady state, which we will use as the performance measure of the algorithm,

for different values of m and the rate. This is depicted in Figure 5-9. The optimal value of

m is the minimum value that achieves a desired steady state performance for a given rate.

The desired steady state performance will depend on the specifics of the application.
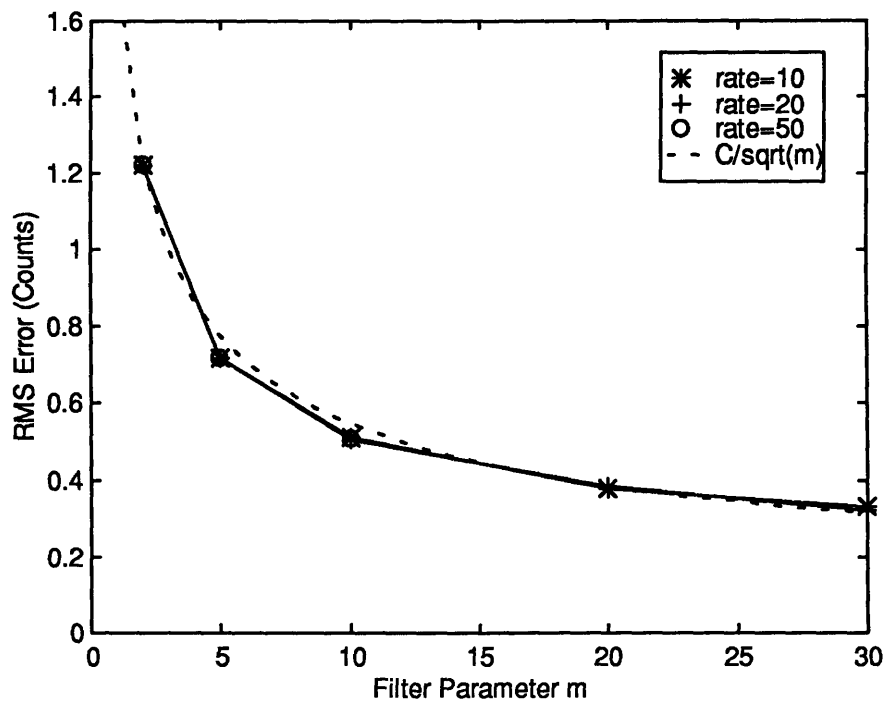
Figure 5-9: Steady state value of error between compensated and original images after
spatial high-pass filter

As is apparent in Figure 5-9, the steady state performance appears to be a function

of the value of m, and not the rate, or temporal correlation, of the sequence of images.

This is not an unexpected result since the spatial autocorrelation of the filtered IRMS

image drops to nearly zero after just a two pixel offset. The consequence of this is that for all the examined rates, the sequence of filtered images is temporally uncorrelated and therefore the performance of the algorithm only depends on the value of m.

The second important characteristic of the steady state performance is the form of the relation between m and the value of σ_{diff}. If we average a number of different scenes, the residual clutter will decrease by the square root of the number of averaged scenes. As illustrated in Figure 5-9, the form of σ_{diff} as a function of m fits the expected form of C/sqrt(m) almost exactly. This implies that for scenes with higher contrast, a higher value of m will be required to achieve a given level of performance. In addition, there will be a limit to the attainable performance, even if the best estimate of the nonuniformity can be constructed. The limit will be a result of the temperature variation in the scene, and the presence of the gain component of the nonuniformity, which will have more of an influence in scenes with larger temperature variations.

In the next section where we examine the performance of the algorithm on real sensor data, there is no uniform image with which to compare the compensated image. Therefore, we must derive performance measures from values we can calculate from the compensated image. Figure 5-10 plots σ_{diff}, which we have been using as the measure of performance, $\sigma_f(m)$, the standard deviation after the temporal high-pass filter and the spatial high-pass filter, and σ_{opt}, the standard deviation of the original scene (without nonuniformity imposed) after spatial high-pass filtering. The trend of both σ_{diff} and $\sigma_f(m)$ is approximately the same, indicating that measuring $\sigma_f(m)$ is a valid measure of the algorithm performance.

This graph also verifies that the compensation is effective. The standard deviation of the compensated image is close to the standard deviation of the original, uniform images after high-pass filtering, σ_{opt}. In addition, the residual nonuniformity, as indicated by σ_{diff}, is small compared to the standard deviation of the compensated image which means that our performance is clutter limited. Since $\sigma_f(m)$ is less than the σ_{opt}, the scene-based algorithm is removing some high frequency clutter, which is not unexpected since part of the estimate of the offset coefficient comes from the current scene. This has implications for the target detection problem. While it may be beneficial to remove clutter, it can also remove some of the target signature, which may harm detection capability.
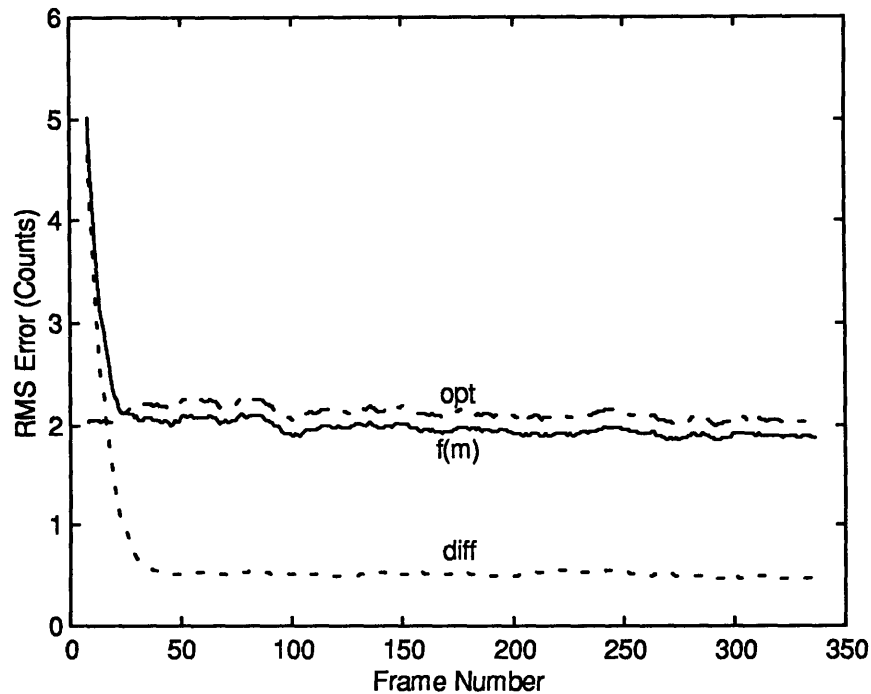
Figure 5-10: Comparison of σ_{diff}, $\sigma_f(m)$, and σ_{opt} as performance measure (standard deviation of uniform sequence before spatial high-pass filter = 6.97 counts)

5.2.3 Applying Algorithm to Skyball Data

The Skyball data were used to evaluate the performance of both the temporal high-pass filter and the source-based techniques. The images used in the analysis were night-time desert scenes, which were obtained from the HgCdTe FPA operating in the MWIR waveband. The frame rate for the system was 30 Hz although every tenth frame was used in this analysis, yielding a frame rate of 3 Hz. Figure 5-11 shows a typical image obtained from the system; the scene detail is completely dominated by sensor nonuniformity.
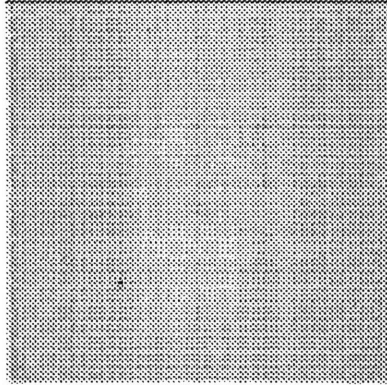
Figure 5-11: Uncompensated image from Skyball sensor

Since there were calibration frames taken prior to imaging the background scene, both the source-based and scene-based compensation techniques can be applied. The results of applying the one-point and two-point source-based compensation and the temporal high-pass filter are shown in Figure 5-12. There are significant improvements in the amount of discernible scene detail after compensation and visually, all three compensation techniques appear to perform equally well.
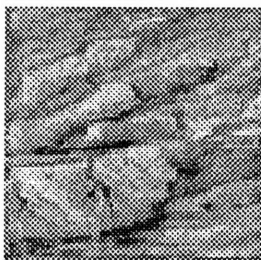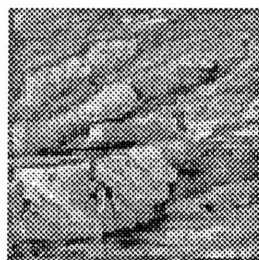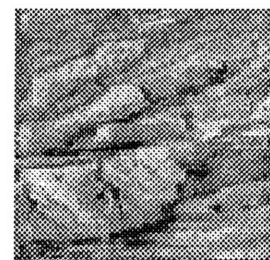
(a)   (b)   (c)

Figure 5-12: Compensated Skyball image after (a) Temporal high-pass filter (m=10), (b) 1-point method (35°C calibration temperature), and (c) 2-point method (20°C and 35°C calibration temperatures)

While both the source and the scene-based algorithms appear to work well qualitatively, a quantitative performance measure of the different techniques is more difficult since there is no ideal reference image for comparison with the corrected images. Instead of differencing the outputs of the different compensation methods, we will compare the standard deviation of the compensated image, after high-pass filtering, with the standard deviation of the high-pass filtered original image (see Figure 5-13) as in the previous section. By filtering the original image with the high-pass filter, we are reducing most of the background clutter, leaving mainly the high frequency nonuniformity. It is expected that the compensation will remove much of the high frequency nonuniformity and therefore the output of the high-pass filter should be due to residual clutter and compensation error.
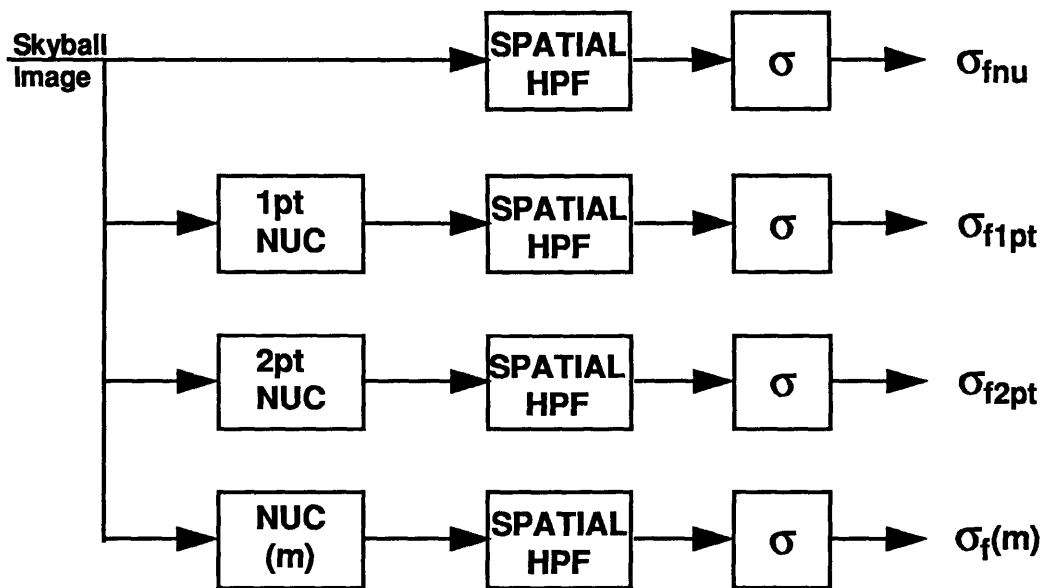

Figure 5-13: Block diagram of performance evaluation

When measuring the standard deviation of the output frames, it is important to exclude any bad pixels in the array. The bad pixels may flicker, always stay on, or always stay off. In order to eliminate the effects of these pixels, a bad-pixel map is constructed using the blackbody calibration frames that precede the desert scenes. In this case, any pixel whose response was more than three standard deviations from the mean response was considered to be bad in all subsequent images. The values of these pixels were not included in the calculations of the standard deviations. In situations where there is no calibration data, the determination of bad pixels is more difficult, however, the bad pixels typically constitute a very small portion of the FPA.

The average value of the standard deviation of the scene, without compensation, but after a spatial high-pass filter, is 1388.2 counts. The standard deviations, after compensation, bad pixel removal, and spatial high-pass filtering were calculated for both the one-point and two-point source-based methods. Figure 5-14 illustrates that both techniques reduce the spatial standard deviation considerably as compared to the original image. The two-point nonuniformity compensation eliminates more of the high frequency components (approximately 98%) than the one-point compensation (approximately 97%); clearly, the percentage difference between the two is very small. While one-point compensation does suppress a significant amount of nonuniformity, it may not be sufficient for the detection of low contrast targets in clutter.
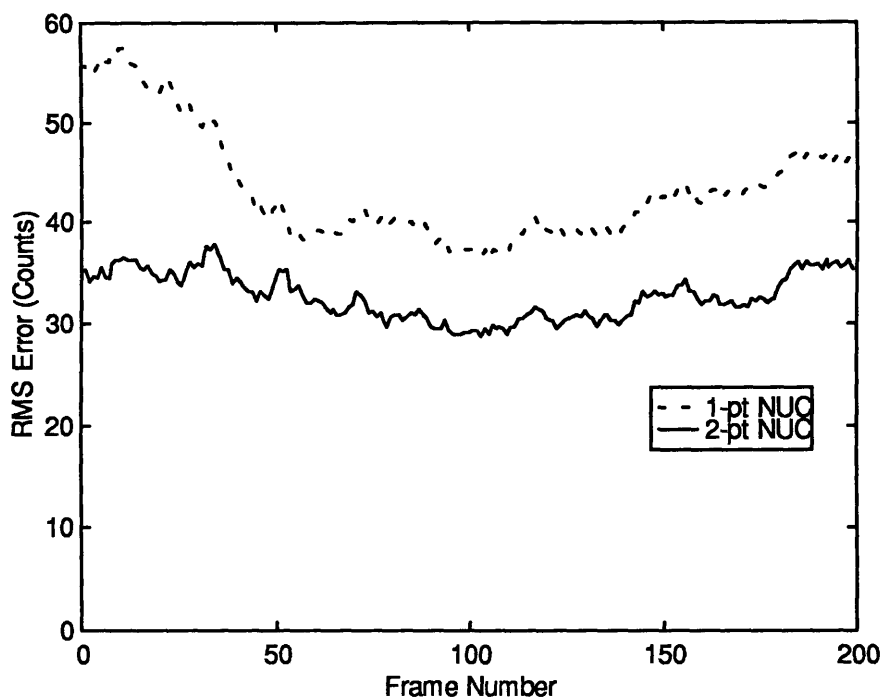
Figure 5-14: Comparison of one-point and two-point compensation for Skyball data

The results of applying the temporal high-pass filter, for three values of m, followed by a spatial high-pass filter are shown in Figure 5-15. As expected from the previous section, the larger the value of m, the more frames are required to achieve the steady state performance.
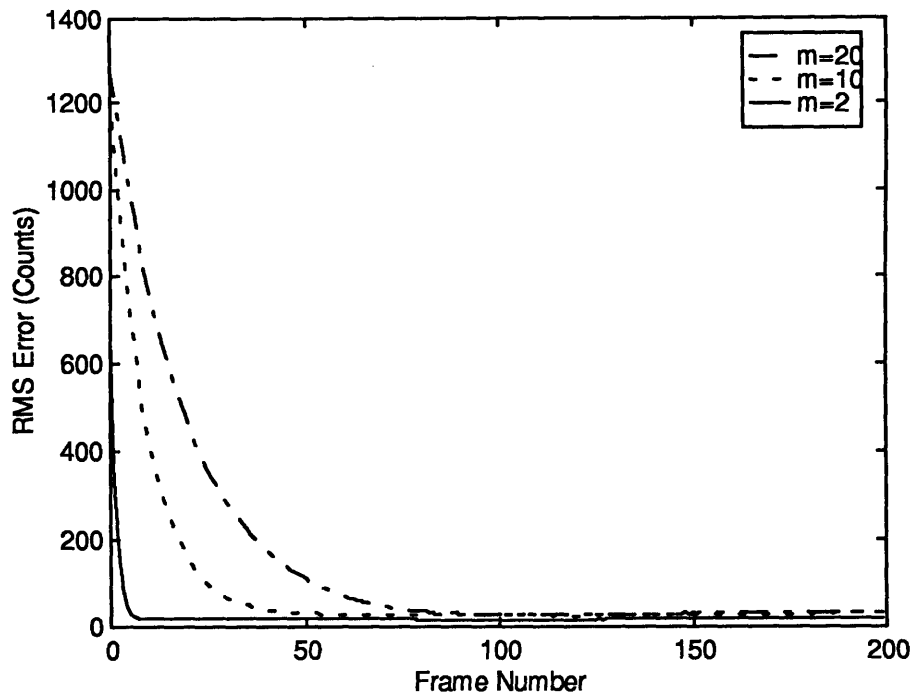
Figure 5-15: Standard deviation of compensated image after temporal and spatial high-pass filters

The steady state performance (i.e., frames 100-200) of the temporal high-pass filter is shown in Figure 5-16. As a reference, the results of the two-point nonuniformity compensation are also included in the figure and the average standard deviation for the uncompensated, high-pass filtered images is 1388.2 counts. It is apparent that after the algorithm has obtained enough frames to make a good estimate of the nonuniformity, the standard deviation of the output image drops considerably.
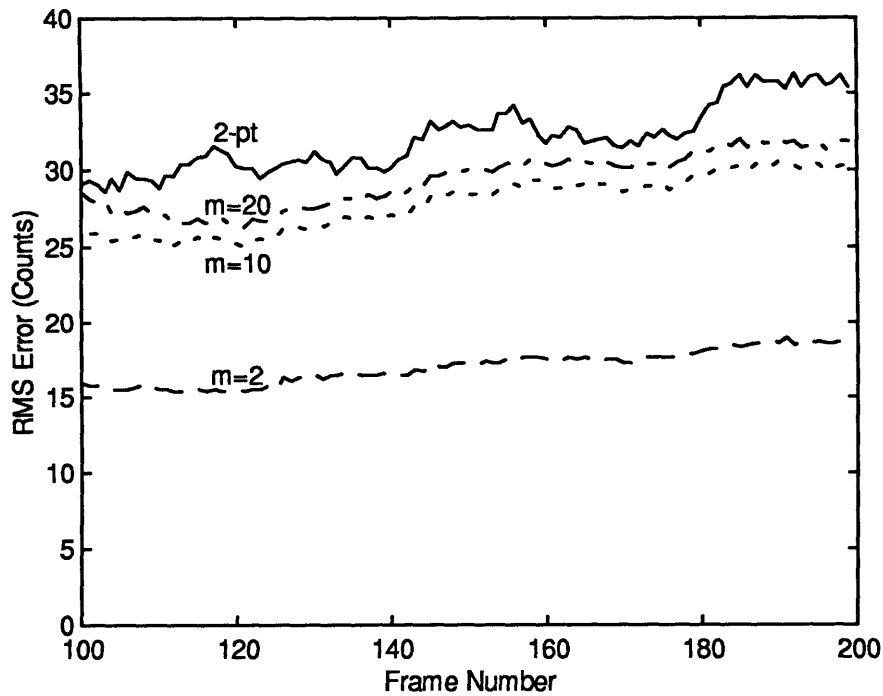
Figure 5-16: Comparison of scene-based compensation and two-point compensation after spatial high-pass filter

The steady state performance indicates that there is additional reduction of the spatial variation using the scene-based techniques. The additional drop in standard deviation is not likely to be due to the effects of high order terms in the nonuniformity, which we have neglected in this thesis, since these results are consistent with those in Section 5.2.2 where we only imposed gain and offset nonuniformities. Therefore, the scene-based algorithm is reducing clutter in the image as well as nonuniformity. As evidenced in Figure 5-16, the smaller the value of m, the more clutter is rejected. For small values of m, more of the current scene is used in the nonuniformity estimate and therefore more of the scene clutter will be eliminated. While it may be of some benefit to reduce the clutter, the consequence is that the targets with the same temporal behavior as

the clutter may be reduced as well. The amount which the target may be reduced and still be detectable will set a lower limit on the value of m. The optimal value of m for a desired performance level cannot be determined without the knowledge of specific target characteristics; the specifics of the detection of low contrast targets in clutter is beyond the scope of this thesis.

6 Conclusion and Summary

This thesis developed scene-based nonuniformity compensation techniques and compared the results to source-based techniques. Nonuniformity characteristics were examined to motivate the need for nonuniformity compensation and to provide an indication of the performance of different techniques (e.g., one-point vs. two-point compensation). Source-based methods were evaluated as a basis for comparison for the scene-based methods.

It was shown that one-point nonuniformity compensation could achieve the performance of two-point compensation only at, or near, the compensation temperature. When applied to blackbodies over a temperature range of 10°C to 45°C, the error after two-point compensation was, on average, 18 times smaller than the error after one-point correction. This means that target intensity would have to be 18 times greater for one-point techniques to achieve comparable detection performance as the two-point techniques. However, for scenes with a small dynamic range about the calibration temperature, one-point compensation may be sufficient.

The performance of the temporal high-pass filter technique, which subtracts a weighted running average of the previous pixel values from the current value, was shown to reduce spatial variance below that of the two-point source-based performance for low contrast scenes, from 43 counts to as low as 17 counts. The reduction in variance was due to both nonuniformity compensation and suppression of scene clutter. While background rejection may be beneficial, it may come at the expense of reducing the target

75

intensity and consequently, target detection capabilities. Therefore, optimal scene-based compensation performance cannot be evaluated independently of target characteristics.

There are a number of issues that could be examined in more depth in a future study. The data sets used in this analysis came from multiple sensors, which prevented a comprehensive model of performance. A full set of data from one FPA would allow for the nonuniformity analysis, as performed in Chapter 3, to be compared directly to the performance of various scene and source-based algorithms.

The analysis for this thesis was performed on scenes with low contrast and high spatial and temporal correlation. A similar analysis on scenes with a variety of spatial and temporal characteristics would provide a more thorough evaluation of these methods.

Finally, the effects of compensation algorithms on target detection were not directly examined. An evaluation of algorithm performance is incomplete without knowledge of target characteristics. Future work could investigate the trade-off between additional clutter rejection in the scene-based techniques and the potential to decrease target detection capabilities.

7 Bibliography

1. Ballingall, R.A. 1990. Review of Infrared Focal Plane Arrays. *SPIE Infrared Technology and Applications* 1320 :70-87.

2. Blumenau, P.M., et al. 1994. Non-uniformity compensation for IR focal plane arrays. Paper presented at IRIS Specialty Group on Passive Sensors, Sandia National Lab, Kirland AFB, Albuquerque.

3. Boreman, G.D. and C. Costanzo. 1987. Compensation for gain nonuniformity in HgCdTe infrared charge-coupled-device focal planes. *Optical Engineering* 26, no. 10 (October): 981-984.

4. Broekaert, M. and B.N. du Payrat. 1994. Nonlinearity and nonuniformity corrections for the IRIS family of IRCCD thermal imagers. *SPIE Infrared Technology XX* 2269: 507-523.

5. Cantella, M.J. 1988. Space Surveillance With Medium-Wave Infrared Sensors. *The Lincoln Laboratory Journal* 1, no. 1: 75-88.

6. Cantella, M.J. 1993. Staring Sensor Systems. In *The Infrared and Electo-Optical Systems Handbook.* Vol. 5, *Passive Electro-Optical Systems*, ed. Stephen Campana, 157-207. Ann Arbor: Infrared Infromation Analysis Center; Bellingham, Wash.: SPIE Optical Engineering Press.

7. Cantella, M.J., et al. 1989. Low-background application of Schottky-barrier IR sensors. *SPIE Optical Sensors and Electronic Photography* 1071: 12-30.

8. Carrison, C.L. and N.A. Foss. 1980. Fixed pattern noise compensation techniques for staring infrared focal planes. *Optical Engineering* 19, no. 5 (September/October): 753-757.

9. Caulfield, J.T., et al. 1993. Performance of Real-Time Adaptive Nonuniformity Correction Techniques for IRFPAs. *Proc. IRIS Passive Sensors* 1: 151-166.

10. Cheung, L., E. Dereniak, and D.Perry. 1988. Computer simulation of spatial nonuniformity correction in a staring sensor. *SPIE Infrared Technology XIV* 972: 65-82.

11. Descour, M. and E. Dereniak. 1992. Functional aspects of the retina relating to infrared focal plane arrays. *SPIE Infrared Detectors and Focal Plane Arrays II* 1685: 110-117.

12. Fenner, J.W., S.H. Simon, and D.D. Eden. 1994. Design of a IRFPA Nonuniformity Correction Algorithm to be implemented as a Real-time Hardware Prototype. *SPIE* 2225: 350-358.

13. Greene, T.F. 1988. Infrared sensor test requirements and critical issues. *SPIE Infrared Scene Simulation: Systems, Requirements, Calibration, Devices and Modeling* 940: 18-24.

14. Greiner, M.E., R.L. Smith, and H.A. Timlin. 1994. Uniformity and stability in 2-dimensional infrared focal plane arrays. *SPIE* 2225: 176-184.

15. Holst, G.C. 1993. Infrared Imaging System Testing. *The Infrared and Electo-Optical Systems Handbook.* Vol. 4, *Elecro-Optical Systems Design, Analysis, and Testing,* ed. Michael C. Dudzik, 195-243. Ann Arbor: Infrared Infromation Analysis Center; Bellingham, Wash.: SPIE Optical Engineering Press.

16. Cincinnati Electronics. 1993. *IRC-160/IRC-160ST User Manual.*

17. Karins, J.P. 1992. Models of nonlinearities in focal plane arrays. *SPIE Infrared Detectors and Focal Plane Arrays II* 1685: 103-109.

18. Kimata, M., et al. 1987. 256x256 element platinum silicide Schottky-barrier infrared charge-coupled device image sensor. *Optical Engineering* 26, no. 3 (March): 209-215.

19. Kosonocky, W.F. 1987. Infrared Image Sensors with Schottky-Barrier Detectors. *SPIE Technologies for Optoelectronics* 869: 90-106.

20. Kruer, M.R., D.A. Scribner, and J.M. Killany. 1987. Infrared focal plane array technology development for Navy applications. *Optical Engineering* 26, no. 3 (March): 182-190.

21. Massie, M.A., et al. 1992. Neuromorphic infrared focal plane performs on-plane local contrast enhancement, spatial and temporal filtering. *SPIE Infrared Technology XVIII* 1762: 361-375.

22. Milton, A.F., F.R. Barone, and M.R. Kruer. 1985. Influence of nonuniformity on infrared focal plane array performance. *Optical Engineering* 24, no. 5 (September/October): 855-862.

23. Mooney, J.M. 1991. Effect of spatial noise on the minimum resolvable temperature of a staring sensor. *Applied Optics* 30, no. 23 (August): 3324-3332.

24. Mooney, J.M., and E.L Dereniak. 1987. Comparison of the performance limit of Schottky-barrier and standard infrared focal plane arrays. *Optical Engineering* 26, no. 3 (March): 223-227.

25. Mooney, J.M., et al. 1989. Responsivity nonuniformity limited performance of infrared staring cameras. *Optical Engineering* 28, no. 11 (November): 1151-1161.

26. O'Neil, W.F. 1992. Dithered Scan Detector Compensation. *Proc. IRIS Passive Sensors* 1:123-134.

27. O'Neil, W.F., et al. 1993. Experimental Performance of a Dither-Scanned InSb Array. *Proc. IRIS Passive Sensors* 1:167-176.

28. Palmer, J.M. 1994. The limits of radiometry. *SPIE Infrared Technology XX* 2269: 592-602.

29. Perry, D.L. 1992. Linear theory of nonuniformity correction in platinum silicide focal plane arrays. *SPIE Infrared Technology XVIII* 1762: 60-69.

30. Perry, D.L. and E.L. Dereniak. 1993. Linear theory of nonuniformity correction in infrared staring sensors. *Optical Engineering* 32, no. 8 (August): 1854-1859.

31. Poropat, G.V. 1989. Nonlinear compensation for responsivity nonuniformities in cadmium mercury telluride focal plane detector arrays for use in the 8 to 12 μm spectral region. *Optical Engineering* 28, no. 8 (August): 887-896.

32. Scribner, D.A., et al. 1991. Infrared Focal Plane Array Technology. *Proceedings of the IEEE* 79, no. 1 (January): 66-85.

33. Scribner, D.A., et al. 1987. Measurement, characterization, and modeling of noise in staring infrared focal plane arrays. *SPIE Infrared Sensors and Sensor Fusion* 782: 147-160.

34. Scribner, D.A., et al. 1990. Nonuniformity correction for staring IR focal plane arrays using scene-based techniques. *SPIE Infrared Detectors and Focal Plane Arrays* 1308: 224-233.

35. Scribner, D.A., et al. 1987. Physical limitations to nonuniformity correction in IR focal plane arrays. *SPIE Focal Plane Arrays: Technology and Applications* 865: 185-202.

36. Scribner, D.A., et al. 1988. Spatial noise in staring IR focal plane arrays. *SPIE Infrared Detectors and Arrays* 930: 56-63.

37. Scribner, D.A., et al. 1989. Test and Evaluation of Stability in IR Staring Focal Plane Arrays After Nonuniformity Correction. *SPIE Test and Evaluation of Infrared Detectors and Arrays* 1108: 255-264.

38. Scribner, D.A., et al. 1991. Adaptive Nonuniformity Correction for IR Focal Plane Arrays Using Neural Networks. *SPIE Infrared Sensors: Detectors, Electronics, and Signal Processing* 1541: 100-109.

39. Scribner, D.A., et al. 1992. An Imaging Metric for Infrared Focal Plane Arrays. *SPIE Test and Evaluation of IR Detectors and Arrays II* 1686:136-144.

40. Shepherd, F.D. and J.M. Mooney. 1987. Design Considerations for IR Staring-Mode Cameras. *SPIE Electro-Optical Imaging Systems Integration* 762: 35-50.

41. Shepherd, F.D. and J.M. Mooney. 1987. Non-uniformity Limited Performance of IR Staring Cameras. *Proc. IRIS Imaging*:141-152.

42. Shumaker, D.L., J.T. Wood, and C.R. Thacker. 1988. *FLIR Performance Handbook*. Alexandria, VA: DCS Corporation.

43. Villiani, T.S., et al. 1989. Construction and Performance of a 320 X 244 - Element IR-CCD Imager with PtSi Schottky-Barrier Detectors. *SPIE Infrared Detectors, Focal Plane Arrays, and Imaging Sensors* 1107: 9-21.

44. Vincent, J.D. 1990. *Fundamentals of Infrared Detector Operation and Testing*. New York: John Wiley and Sons.

45. Wolfe, W.L. and G.J. Zissis, eds. 1985. *The Infrared Handbook*. ERIM IR Information and Analysis Center for Office of Naval Research.